

**STUDY ON THE SIMULTANEOUS HYDROPHILICITY/OLEOPHOBICITY OF AN
IONIC LIQUID THIN FILM**

by

Victor Alejandro Manrique

B.S. in Chemical and Biomolecular Engineering, The Georgia Institute of Technology,
2012

Submitted to the Graduate Faculty of
Swanson School of Engineering in partial fulfillment
of the requirements for the degree of
Master of Science

University of Pittsburgh

2016

UNIVERSITY OF PITTSBURGH
SWANSON SCHOOL OF ENGINEERING

This thesis was presented

by

Victor Alejandro Manrique

It was defended on

June 27, 2016

and approved by

Susan Fullerton, Ph.D., Assistant Professor, Department of Chemical and Petroleum
Engineering

Sachin Velankar, Ph.D., Associate Professor, Department of Chemical and Petroleum
Engineering

Thesis Advisor: Lei Li, Ph.D., Assistant Professor, Department of Chemical and Petroleum
Engineering

Copyright © by Victor Alejandro Manrique

2016

STUDY ON THE SIMULTANEOUS HYDROPHILICITY/OLEOPHOBICITY OF AN IONIC LIQUID THIN FILM

Victor Alejandro Manrique, M.S.

University of Pittsburgh, 2016

Simultaneous hydrophilic/oleophobic materials are desired for various applications where anti-fogging is required. The ideal coating would be one that can be applied physically, such as an ionic liquid (IL) thin film. This thesis project explores the simultaneous hydrophilic/oleophobic wetting behavior of a thin film of 1-ethyl-3-methylimidazolium bis(trifluoromethylsulfonyl)imide (EMIIm) on silica substrate. First, atomic force microscopy revealed that EMIIm forms a complete film on silica substrate with film dewetting occurring at 1.1 ML (monolayer thickness). Next the molecular arrangement was analyzed with angle-resolved x-ray spectroscopy, by calculating the atomic ratio of nitrogen from the anion to nitrogen from the cation (N^-/N^+). For the three samples tested the ratio was above 0.5, indicating that the anion was organized over the cation even when the film was dewetted. This was determined to be due to the planar structure of the EMI cation. Further analysis done by changing the takeoff angle revealed a change in N^-/N^+ for 0.6 ML thin film; N^-/N^+ for the film bulk and the film surface was 0.8 and 0.9 respectively. This meant that at 0.6 ML the ions are in a layered arrangement with the fluorinated anion layer at the surface. Finally, it was found that while the water contact angle (WCA) was low for all film thickness values tested (avg. $5.33^\circ \pm 3.91$) the hexadecane contact angle (HCA) plateaued to 41.15° for samples with thickness greater than 0.7 ML. Time-dependent HCA trials were conducted, for 24 hours and 3 hours. The trials confirmed that film penetration was occurring, as the HCA reached a final equilibrium value

after 3 hours. The contact liquid is drawn to the high energy silica, so the liquid will pass through the intermolecular holes in the film to get to the substrate. Given that the WCA is low and constant, and the size difference between water and hexadecane, the hole size must be between 0.3 nm and 0.8 nm. In addition, the final HCA had a positive correlation to the film thickness.

TABLE OF CONTENTS

PREFACE.....	XI
1.0 INTRODUCTION.....	1
1.1 IONIC LIQUIDS	1
1.2 WETTING PHENOMENA	4
1.3 OBJECTIVE	5
2.0 LITERATURE REVIEW.....	6
2.1 IONIC LIQUID THIN FILMS.....	6
2.2 CONTACT ANGLE	10
2.3 SIMULTANEOUS HYDROPHILICITY/OLEOPHOBICITY	13
3.0 METHODOLOGY.....	18
3.1 MATERIALS	18
3.2 EXPERIMENTAL PROCEDURE	21
3.3 UV/O₃ CLEANING	21
3.4 DIP COATER	22
3.5 ELLIPSOMETRY	23
3.6 GONIOMETER.....	26
3.7 OPTICAL MICROSCOPY	28
3.8 ATOMIC FORCE MICROSCOPY.....	29

3.9	X-RAY PHOTOELECTRON SPECTROSCOPY (XPS)	31
4.0	RESULTS AND DISCUSSION	34
4.1	TOPOGRAPHY OF EMIIM THIN FILM	34
4.2	MOLECULAR ARRANGEMENT OF EMIIM THIN FILM	45
4.3	WETTABILITY OF EMIIM THIN FILM.....	51
5.0	CONCLUSION.....	64
APPENDIX A		67
ELLIPSOMETRY DATA FOR EMIIM THIN FILM		67
APPENDIX B		69
TOPOGRAPHY OF IONIC LIQUID THIN FILMS		69
APPENDIX C		73
DYNAMIC CONTACT ANGLE ANALYSIS OF EMIIM THIN FILM		73
BIBLIOGRAPHY		78

LIST OF TABLES

Table 1: Properties and Vendors of Ionic Liquids Utilized	19
Table 2: Chemical Structures of Ionic Liquids Utilized	20
Table 3: Roughness analysis for bare silica and EMIIIm thin film	43
Table 4: ARXPS spectra (N 1s) fitting calculations for EMIIIm thin film.....	46
Table 5: 24-hour HCA Exponential Fit Parameters.....	59
Table 6: 3-hour HCA Exponential Fit Parameters.....	63
Table 7: Ellipsometry Data for EMIIIm Solution 0.01, 0.1, 0.2, 0.25 g/L.....	67
Table 8: Ellipsometry Data for EMIIIm Solution 0.3, 0.5, 0.75 g/L.....	68
Table 9: Ellipsometry Data for EMIIIm Solution 1.0, 5.0 g/L.....	68
Table 10: Film Thickness for MOEDEA, EMZIA, and EMIIIm, for 1.0 g/L	69
Table 11: Advancing HCA for EMIIIm thin film on silica.....	73

LIST OF FIGURES

Figure 1: Chemical structure of various cations and anions of ionic liquids. This image was copied from reference 2 (This is an unofficial adaptation of an article that appeared in an ACS publication. ACS has not endorsed the content of this adaptation or the context of its use.).....	2
Figure 2: Schematic of DMPIIm on silica, showing dewetting occurring as the thickness increases. Reproduced from Ref 17 with permission of The Royal Society of Chemistry.	10
Figure 3: a) Schematic of advancing contact angle. The advancing contact angle is the angle measured after the droplet moves (8); b) Schematic of receding contact angle. The receding contact angle is the angle measured as soon as the droplet moves (3). Reprinted with permission from Gao, L. and T.J. McCarthy, <i>Contact Angle Hysteresis Explained</i> . Langmuir, 2006. 22(14): p. 6234-6237. Copyright 2016 American Chemical Society.	12
Figure 4: Chemical structures of ZDOL, Z-tetraol, and Z-03. Reproduced from Ref 23 with permission of The Royal Society of Chemistry.	15
Figure 5: Schematic of penetration of ZDOL film by water and hexadecane. Reproduced from Ref 23 with permission of The Royal Society of Chemistry.	16
Figure 6: UV/Ozone ProCleaner.....	22
Figure 7: KSV-DCX2 Dip Coater.....	23
Figure 8: alpha-SE Ellipsometer.....	24
Figure 9: a) Cauchy Model Parameter Interface;.....	26
Figure 10: VCA optima XE Goniometer	27
Figure 11: Zeiss Axio Lab Optical Microscope.....	28
Figure 12: Veeco Manifold Multimode V- Dimension V Combination SPM.....	30
Figure 13: EMIIIm film thickness vs. dip coating-solution concentration, with a linear trendline	35

Figure 14: Optical images of EMIIIm film on silica, of thickness 0.6, 1.1, and 1.7 ± 0.1 ML	38
Figure 15: AFM topography images of EMIIIm film on silica, of thickness 0.6, 1.1, and 1.7 ± 0.1 ML.....	40
Figure 16: AFM section analysis of EMIIIm film on silica, of thickness 0.6, 1.1, and 1.7 ± 0.1 ML.....	42
Figure 17: a) Structure, monolayer thickness of DMPIIm ¹⁷ ; b) Structure, monolayer thickness of EMIIIm	45
Figure 18: ARXPS spectra (N 1s) of EMIIIm thin film of thickness 0.6, 1.1, and 1.7 ML, at 0° and 60° takeoff angle	47
Figure 19: EMIIIm layered structure. The anion (yellow sulfur, pink fluoride) is near the film surface, while the cation (black carbon) forms the initial layer.....	50
Figure 20: Static contact angle data with standard deviation for various ionic liquid thin films	52
Figure 21: Static WCA and HCA for EMIIIm thin film with standard deviation, WCA average line, and HCA plateau line.....	54
Figure 22: 24-hour HCA data trend for EMIIIm thin film, with exponential fit, linear trendline (0.3 ML), and PTFE control trend with linear trendline.....	58
Figure 23: 3-hour HCA data trend for EMIIIm thin film, with exponential fit and PTFE control trend	62
Figure 24: Optical images of MOEDEA, EMZIA, and EMIIIm film on silicon wafer, all solution 1 g/L	70
Figure 25: AFM Topography images of MOEDEA, EMZIA, and EMIIIm film on silica, all solution 1 g/L	72
Figure 26: Advancing Contact Angle graphs for EMIIIm film	74
Figure 27: Receding HCA for EMIIIm film 0.6, 1.1 ML	76

PREFACE

The author would like to thank Dr. Lei Li for invaluable guidance in the assembly of this thesis. The author would also like to thank Dr. Andrew Kozbial for procedural training, software training, and valuable discussion.

1.0 INTRODUCTION

1.1 IONIC LIQUIDS

Ionic liquids (ILs) have been defined in a 2000 NATO meeting as a subset of molten salts with melting points below 373K ¹. IL research had been going strong long before then, ever since Walden published his findings on the conductivity of ethylammonium nitrate (EAN) in 1914 ². Ionic liquids possess many unique properties due to the chemical structure of the cation and anion. In general, the cation and anion are structured in a way that disrupts lattice packing; this is what prevents the IL from solidifying. Cations have low symmetry in their structure; they usually feature a positively charged nitrogen or phosphorous center. Anions are weakly basic compounds with a diffuse or protected negative charge; they can range from halides to heavily fluorinated compounds. A sample of common ionic liquid cations and anions are shown in Figure 1.

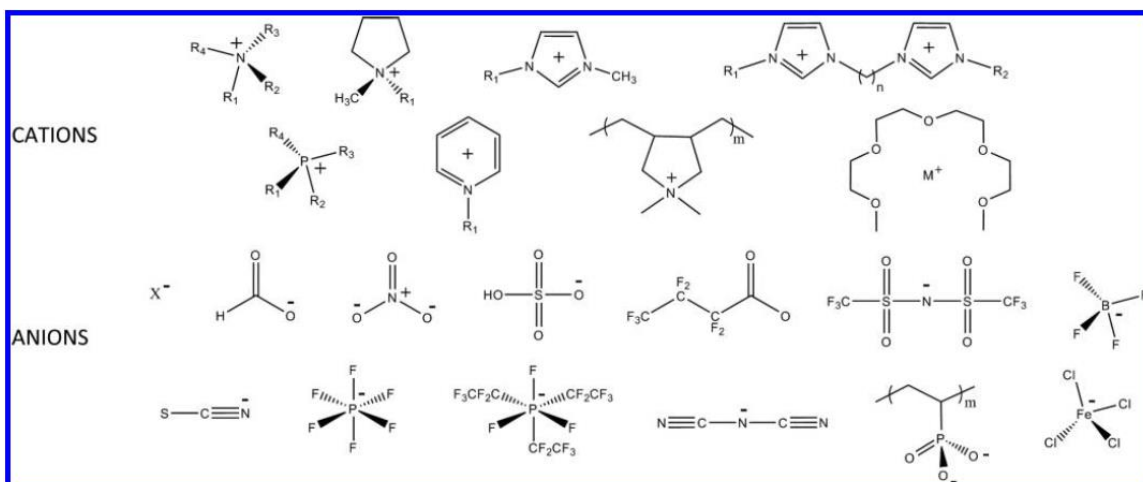


Figure 1: Chemical structure of various cations and anions of ionic liquids. This image was copied from reference 2 (This is an unofficial adaptation of an article that appeared in an ACS publication. ACS has not endorsed the content of this adaptation or the context of its use.)

Ionic liquids have been studied extensively for a host of applications. The high conductivity of ILs makes them ideal for electrochemical processes. Studies range from using ILs as an electrode coating for heavy metal detection ³, forming carbon composite/carbon paste electrodes (CPE) with an IL component ⁴, and using an IL as the electrolyte in the electrodeposition of Al from a water-free AlCl_3 solution ⁵. Various properties of ionic liquids also make them very attractive for use as solvents in reaction systems. ILs are known for dissolving a wide range of organic and inorganic compounds, including polar compounds, allowing for a range of reagent combinations. At the same time ILs are immiscible with a number of common organic solvents, opening up the possibility of a unique two-phase system, one with a polar phase and a nonpolar phase ⁶. Finally, ionic liquids are nonvolatile and thermally stable, leading to easy separation via distillation ⁷. All of these factors have driven research into the use of ILs in synthesis reactions. such as the hydrolyzation of cyclohexene via a cationic “Osborn complex” ⁸, or the use of ILs in the epoxidation of 2,2-dimethylchromene with a chiral Mn^{III} complex ⁹.

One unique area of ionic liquid research is ionic liquid thin films. Ionic liquids exhibit unique properties when confined to a solid substrate. Of primary interest is the molecular arrangement of the ions. This arrangement affects properties such as film thickness, film topography, and film stability (i.e. how easy is it to disrupt the film). The curious thing is the ease with which the arrangement can be changed, just by changing ions, side chains, or the substrate. Already IL thin films are being explored for applications in lubrication, analytical instruments, catalysis, and many others ¹⁰. A study of IL thin film on steel revealed that the friction coefficient of the film decreases with increasing alkyl side chain length ¹¹. Simple changes to the ion structure can have a big impact on the thin film property. Despite the depth of work already available concerning IL thin film, there is a distinct lack of data on the wettability of IL thin film. It is unknown under what circumstances is IL thin film hydrophilic or oleophobic. By examining the known data on IL thin film formation, it would seem that IL thin film can have a similar arrangement as other coatings that exhibit simultaneous hydrophilicity/oleophobicity.

1.2 WETTING PHENOMENA

The wetting of surfaces by a liquid droplet is an important parameter that reveals much about a surface's properties. Wetting is directly tied to the surface energy, and as such is influenced by surface homogeneity and purity. Moreover, it is a simple phenomenon to observe and measure. One important research topic concerning wettability is the design of surfaces more wettable to water than to oil. Such a surface is highly desirable due to the myriad of applications that can arise from that. Such a surface could be used to prevent fogging on items such as glasses, windows, and analytical instruments ¹². Fogging occurs due to droplets forming on the surface. These droplets interfere with light transmission, decreasing the efficiency of surfaces that depend on light passing through. If the surface is wettable to water, then no droplets will form and no fogging occurs. Coatings such as multilayer nanoporous silicate, TiO₂-based nanoparticle coatings, and polyelectrolyte plasma polymer substrates coated with ionic amphiphilic fluoro-surfactants have proven to be highly hydrophilic ¹². The main issue with these coatings is contamination. As these coatings have high surface energy, hydrocarbons in the air as well as water will spread on the coating once they come into contact with the coating. As more hydrocarbons spread on the coating a film of oil forms on the coating, leading to fogging once more. This limits the time frame in which these surfaces are useful. A simultaneously hydrophilic/oleophobic surface could not only prevent fogging but also prevent contamination, ensuring longevity.

1.3 OBJECTIVE

The structure and assembly of various ionic liquids close to various solid substrates has been explored in depth. However, there is a lack of understanding of the wettability of ionic liquid thin films. Based on what is known about the formation of IL thin film there is strong evidence that an IL thin film would be an ideal coating that can exhibit simultaneous hydrophilicity/oleophobicity. The objective of this thesis is to study the wettability of a thin film 1-ethyl-3-methylimidazolium bis(trifluoromethylsulfonyl)imide (EMIIIm) on silica surface. This was done by fabricating IL thin films by dip coating and analyzing wettability to distilled water and hexadecane via sessile drop method. To fully understand the wetting behavior of EMIIm thin film the film topography was analyzed. Film thickness was measured via ellipsometry. Film topography was visualized and analyzed via optical microscopy and atomic force microscopy (AFM). Molecular arrangement of the film was analyzed via angle resolved x-ray photoelectron spectroscopy (ARXPS). Finally, in addition to standard static contact angle measurement the hexadecane contact angle (HCA) was measured over a period of time to observe any changes in the HCA value.

2.0 LITERATURE REVIEW

2.1 IONIC LIQUID THIN FILMS

The interaction between particles, from liquid molecules to solid surfaces, is described by van der Waals forces and electric double layer forces. However, these two theories fail at the intermolecular level. Both van der Waals and double layer are dependent on bulk properties such as density and dielectric permittivity; at the nano-scale these properties are wildly different compared to the bulk. Liquid molecules pressed to a solid surface are formed into quasi-discrete layers by a collection of forces present at close range. These forces are known as solvation forces, and the layers are referred to as solvation layers. The way the solvation layers form varies based on molecular structure and solid surface properties. Solvation layers do not depend on electrostatic forces, rather only geometric arrangement. This includes the structure of the liquid molecule (chirality, symmetry, flexibility) and the structure of the solid surface (roughness, lattice arrangement)¹³. Solvation layers of ionic liquids have unique and interesting properties. They are highly ordered alternating layers of cations and anions. Force vs depth data from AFM tip interaction shows discrete layers via jumps in force response at certain intervals; the range of the intervals, the distance between one layer and the next, and the magnitude of the force response, all depend on the ionic liquid and the solid substrate. For example, IL layers on mica and Au (1 1 1) are in general well defined, with clear jumps in the force profile at a certain

distance. IL layers on silica and graphite however are less well defined, appearing as smeared lines due to the roughness of silica and the tip-substrate interaction of graphite. On mica IL layer number decreased as the cation alkyl chain length increased; this was due to the increased rotation possible with a longer alkyl chain, which meant that it was more favorable for the cation to remain in the bulk phase. On both mica and silica aprotic ILs such as EMIm TFSA and EMIm Ac showed clear ion layer alternation, with the layer distances matching the ion pair diameters ¹⁰. Finally, sum frequency generation spectroscopy showed that for imidazolium cations on silica, the alkyl chains influence the orientation of the imidazolium ring on the silica substrate; decreasing the alkyl chain length lead to a parallel ring orientation with respect to the substrate ¹⁰.

As hinted at in the force-depth graphs there is a limit to the number of solvation layers formed by ionic liquids. Investigation of several IL film samples on various substrates revealed that the topography could range from smooth flat films to a surface dewetted with IL droplets. At first it was thought that a substrate needed to have a surface charge, like mica, in order to create a smooth thin film ¹⁴. This was later thrown into doubt when layering failed to occur on mica when under a vacuum ¹⁵. A study by Gong, et al. found the IL layering mechanism on mica by heating the mica and/or exposing it to UV radiation ¹⁶. Mica in contact with an effective electrolyte, like water from ambient air, would lose its surface K^+ ions via dissociation. This leads to an overall negative surface charge, one that could attract a layer of positive cations and lead to an extended layered arrangement. Untreated freshly cleaved mica would absorb water from ambient air, resulting in a smooth thin film of ionic liquid (1-butyl-3-methylimidazolium tris(pentafluoroethyl) trifluorophosphate (BMIM-FAP) in this study) due to the negative surface charge. Heating the mica would remove the water. ATR-FTIR and contact angle tests showed

that the surface was now heavy with adsorbed hydrocarbons, resulting in a neutral surface. This leads to the initial cation layer to be less bound to the substrate, which leads to dewetting as now the ions favor a random bulk arrangement over a layered arrangement. AFM imaging confirmed the dewetted topography; IL droplets were seen on the heated mica samples. Exposing the mica to UV radiation would remove the hydrocarbons. This would lead to water being absorbed once more on the surface of the mica. Once more the BMIM-FAP thin film on mica would be smooth, not dewetted. Further study by the same group explored IL layering on silica, a substrate with a weaker negative surface charge than mica ¹⁷. 1,2-Dimethyl-3-propyl-imidazolium bis(trifluoromethylsulfonyl)imide (DMPIIm) was found to form both a smooth film as well as a dewetted film on silica. Unlike mica, this change in film topography was seen without any modification to the silica substrate. Here the change was due to film thickness. Film thickness in this study was reported as a ratio of the actual thickness to monolayer thickness (ML). The monolayer thickness is the thickness of one full layer of cation and anion, estimated by using bulk density to calculate molecular size. For DMPIIm 1 ML is equal to ~0.78 nm. Monolayer thickness is a useful starting point for visualizing molecular arrangement. In theory a film with ML value less than one should show incomplete coverage. However, the calculation for ML assumes a cubic arrangement with ions of equal size; it does not take into account the various steric arrangements that the ions could undertake in order to form a complete layer. This is the case with DMPIIm. AFM images of films ranging from 0.5 ML to 1.3 ML thickness show complete coverage of the substrate. A review of the DMPI cation shows that the cation is roughly planar. As such the cation can arrange into layers onto the weakly negative substrate, leading to complete coverage. However, AFM images also showed dewetting on the film, starting with film thickness of 0.9 ML (~ 0.70 nm). This was judged to be due to a change in the

dominant force present in this IL-substrate interaction. At low thickness the silica-ionic liquid electrostatic interaction is dominant. The cation is drawn to the weakly negative surface and arranges into layers in order to maximize contact with the substrate. This leads to a layered arrangement at first. As the thickness increases, however, the surface charge is screened due to the various IL layers, decreasing its influence on ions in the bulk. The attraction between the ions becomes greater than the substrate attraction, which in the end results in dewetting at a certain critical thickness. This is visualized in Figure 2. Of final note is the use of ARXPS to determine the molecular arrangement. Here the atomic ratio of nitrogen from the imide anion to the nitrogen from the imidazolium cation (N^-/N^+) was used to determine the arrangement; a N^-/N^+ close to 0.5 meant that the arrangement was random, as this matched the stoichiometric ratio of anion nitrogen to cation nitrogen (1:2). In addition, the change in N^-/N^+ as the transmission angle was changed was observed; angle change was used to compare the arrangement in the film bulk to the film surface. It was found that for the film bulk N^-/N^+ was ~ 0.55 for films of 0.5, 0.9, and 1.3 ML thickness; as a whole DMPIIm film on silica was randomly arranged. However, for 0.5 ML the N^-/N^+ ratio was 1.11 as the transmission angle was increased to 60° ; on the surface the 0.5 ML film was primarily anion, indicating a layered arrangement. The N^-/N^+ ratio stayed constant for the other two samples. The main difference was that the other samples, 0.9 ML and 1.3 ML, showed dewetting on the surface in AFM images. This proves that smooth film corresponds to anion-cation layers, while dewetting is associated with random arrangement ¹⁷.

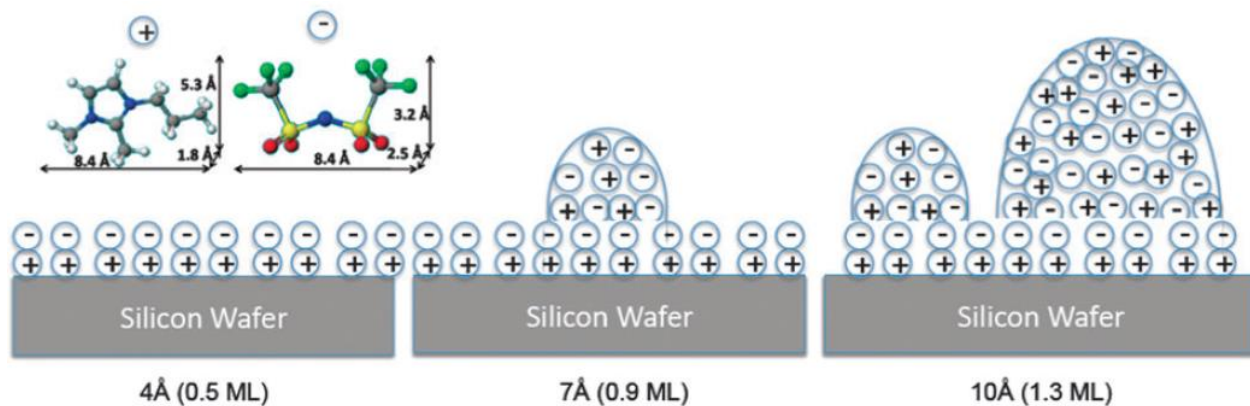


Figure 2: Schematic of DMPIIm on silica, showing dewetting occurring as the thickness increases. Reproduced from Ref 17 with permission of The Royal Society of Chemistry.

2.2 CONTACT ANGLE

When a liquid comes into contact with a (solid) surface it takes on a conformation that minimizes the interfacial energies involved in the liquid-solid interaction. The ideal liquid-solid system is described by Young's Equation:

$$\gamma_{LV} \cos \theta = \gamma_{SV} - \gamma_{SL}$$

γ_{LV} is the liquid- vapor interfacial tension i.e. the liquid surface tension, θ is the equilibrium static contact angle (Young's contact angle) between the liquid and the surface, γ_{SV} is the solid- vapor interfacial tension, and γ_{SL} is the solid-liquid interfacial tension. A smaller contact angle means increased wettability, and the reverse also holds ¹⁸.

Again, Young's Equation describes an ideal contact scenario; the surface is an ideal homogenous surface with one uniform surface energy, so there is one liquid contact shape (i.e. one contact angle) that minimizes the total interfacial energy. In truth physical and chemical variations along the surface create areas of high and low surface energy. The liquid still needs to conform to a shape that minimizes the interfacial energy but now the shape may not have a single uniform contact angle. Surface heterogeneity creates differences between the observed contact angle and the actual contact angle. One example of this difference comes from surface roughness. Defects on a rough surface can affect the configuration of the droplet on the surface; observed angle higher than 90° will actually be lower. The true contact angle is given by Wenzel's Roughness Equation:

$$\cos(\theta_A) = r \cos(\theta_T)$$

θ_A is the observed contact angle, r is the ratio of the true surface area to the geometric area of measurement (known as Wenzel's roughness), and θ_T is the contact angle on an ideal surface. Roughness plays an important role when designing oleophobic/hydrophilic surfaces ¹².

Another factor to consider is the motion of the liquid. Again, in the ideal case the liquid reaches one stable equilibrium shape. In practice the liquid is in flux between several metastable states. The liquid moves to better minimize the total interfacial energy. To properly characterize this phenomena, the dynamic contact angle needs to be obtained. The advancing contact angle is the maximum contact angle obtained as the liquid expands. It is measured by expanding a droplet until motion is detected. The receding contact angle is the minimum contact angle obtained as the liquid retracts. the receding angle is measured by withdrawing fluid from the droplet until movement is detected. In both cases the movement is due to the imbalance between

the surface tension for the liquid and the surface energy for the surface; the difference in energy is converted into movement for the droplet. A schematic is shown in Figure 3. Both angles are angles for which there is a local minimum in Gibbs Free Energy. The difference between the advancing and receding angle is defined as the hysteresis:

$$H = \theta_A - \theta_R$$

θ_A is the advancing contact angle and θ_R is the receding contact angle. The calculated hysteresis is only valid when the advancing and receding angles are taken at the same flow velocity. Keeping the flow velocity of liquid dispensing/withdrawal to as low a value as possible keeps the measured angles close to an “ideal” static angle. It is the difference between these two “ideal” angles that yields the true hysteresis. For an ideal homogenous solid surface the hysteresis would be zero; with no high and low surface energy areas there is nothing to hinder the motion of the liquid, so the advancing angle would equal the receding angle¹⁸.

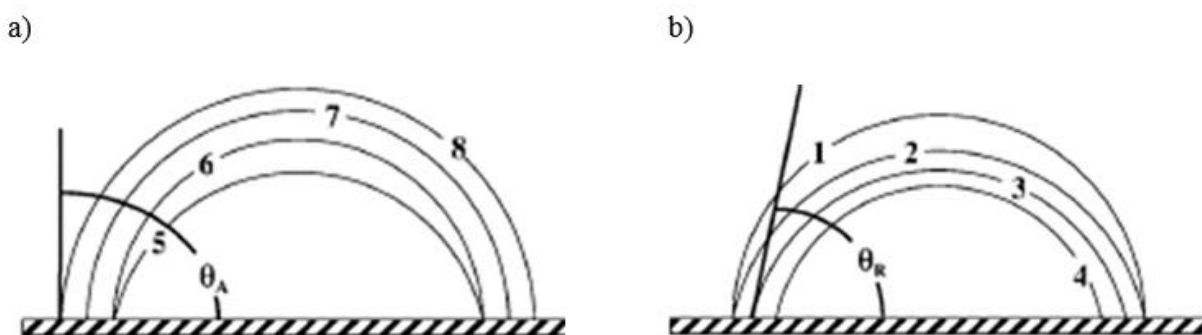


Figure 3: a) Schematic of advancing contact angle. The advancing contact angle is the angle measured after the droplet moves (8); b) Schematic of receding contact angle. The receding contact angle is the angle measured as soon as the droplet moves (3). Reprinted with permission from Gao, L. and T.J. McCarthy, *Contact Angle Hysteresis Explained*. Langmuir, 2006. 22(14): p. 6234-6237. Copyright 2016 American Chemical Society.

For general contact angle measurements an experimentally observed contact angle θ can be used, and for greater accuracy an experimentally measured θ_A can be taken as the “true”/ideal θ . Experimental data shows that θ increases γ_{LV} ¹⁹. Knowing that the surface tension of oils such as hexadecane are lower than the surface tension of water, it stands to reason that the equilibrium contact angle (CA) of oils should be lower than the CA of water. Indeed, this is the case for many surfaces²⁰.

2.3 SIMULTANEOUS HYDROPHILICITY/OLEOPHOBICITY

There has been much development in the field of wetting manipulation. Work has evolved beyond the extremes of superhydrophobic and superhydrophilic surfaces. The goal now is to create “smart” surfaces, a surface that can respond to a changing environment. Part of this includes anti-fog surfaces and self-cleaning surfaces. To prevent fogging on a surface the surface needs to be wettable to water i.e. the contact angle (CA) between the surface and water needs to be low enough to prevent the formation of water droplets. The threshold advancing CA is around 40°¹². The reason for wanting a water film on a surface instead of droplets is that droplets cause light scattering, whereas there is no scattering with a water film. Current anti-fogging coatings are limited by oil contamination. Again, since the surface tension of oils are lower than the surface tension of water the CA of oils will be lower than the CA of water. As such a hydrophilic surface can be wetted by oils with ease. Now the oil contaminated surface will promote water droplets, leading to fogging. Moreover, the oil contaminant is not easily removed due to their low surface energy. The goal of a simultaneous hydrophilic and oleophobic surface is to overcome this. On a simultaneous hydrophilic and oleophobic surface the CA of

oils is lower than the CA of water. There is a driving force for water to displace the oil from the surface. In energy terms the energy gained from water-surface interaction must be greater than the energy lost from breaking the oil-surface interaction ¹².

There are a few examples of simultaneous hydrophilic/oleophobic surfaces. The bulk are the amphiphilic coatings on a hydrophilic surface. For example, Lampitt and Crowther found that a complex of cationic fluoro-surfactants to a maleic anhydride plasma polymer surface was both hydrophilic and oleophobic; the water CA (WCA) was 22° while the hexadecane CA (HCA) was 79° ²¹. The reason for this is a combination of the outward facing perfluoro-alkyl chains, and plasma induced crosslinking that occurs during deposition. The crosslinking prevents the penetration of fluoro-surfactants to the subsurface; as such, while oils like hexadecane are repelled by the perfluoro-alkyl heads, water can pass them and get to the hydrophilic subsurface. Complexes without the crosslinking, such as spin cast poly(ethylene-alt-maleic anhydride) copolymer, repel both hexadecane and water (HCA measured at 81° and WCA measured at 105°), as now both the surface and subsurface is covered in fluoro-surfactants. Howarter and Youngblood found another material, an isocyanate-silane modified silica substrate that binds to a perfluorinated polyethylene glycol oligomers (f-PEG) ²². 24 hours after the reaction of the modified substrate and f-PEGs the WCA was 30°/0° and the HCA was 79°/67°. The key was that water could wet the PEG segments while hexadecane could not wet the perfluorinated segments. In essence the water molecules only “saw” the PEG segments while the hexadecane only “saw” the perfluorinated branches.

Two studies explored the simultaneous oleophobicity/hydrophilicity of a perfluoropolyether (PFPE) thin film on silica ^{20, 23}. The structures of the PFPEs known commercially as ZDOL, Z-tetraol, and Z-03 (Solvay Solexis Inc.) are shown in Figure 4.

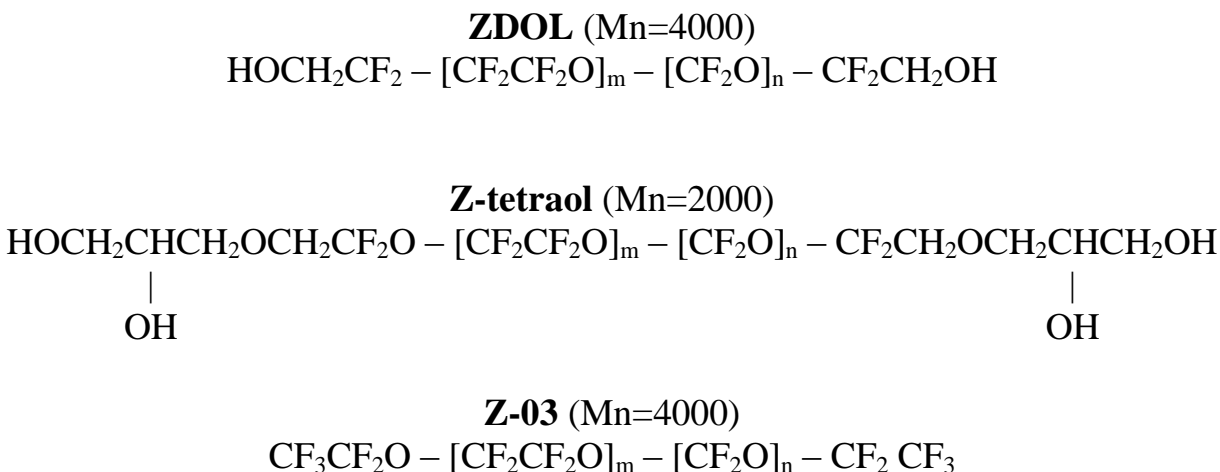


Figure 4: Chemical structures of ZDOL, Z-tetraol, and Z-03. Reproduced from Ref 23 with permission of The Royal Society of Chemistry.

By conducting static and time-dependent HCA trials, and comparing the results to Z-tetraol and Z-03 the mechanism behind the wetting behavior of ZDOL thin film was uncovered. The key is the interaction between the polymer and the substrate. The hydroxyl group on ZDOL is strongly attracted to the silica. This leads to two important facts. First, the molecules will orient themselves so that the hydroxyl group is close to the silica surface, leaving the fluorinated backbone on the top of the film. The strength of the hydroxyl group binding prevents an easy reorientation of the molecules; while the fluorinated backbone may not favor contact with hexadecane, the force generated by the repulsion is not as strong as the binding force. The second fact is that with the polymer strongly bound to the surface, the film created will be tightly packed, with little free space. These two facts, a rigid orientation and a tightly packed film, lead to the observed simultaneous oleophobicity/hydrophilicity²³. The fluorinated backbone repels hexadecane, leading to the initial high oil contact angle. However, hexadecane is simultaneously drawn to the high energy silica substrate. With time the oil will penetrate the film, leading to a decrease in oil contact angle over time. Water, on the other hand, has a low contact angle right at

the start. It too is drawn to the silica, but unlike hexadecane it can penetrate the film much more easily because it is not as bulky as the oil. This is visualized in Figure 5.

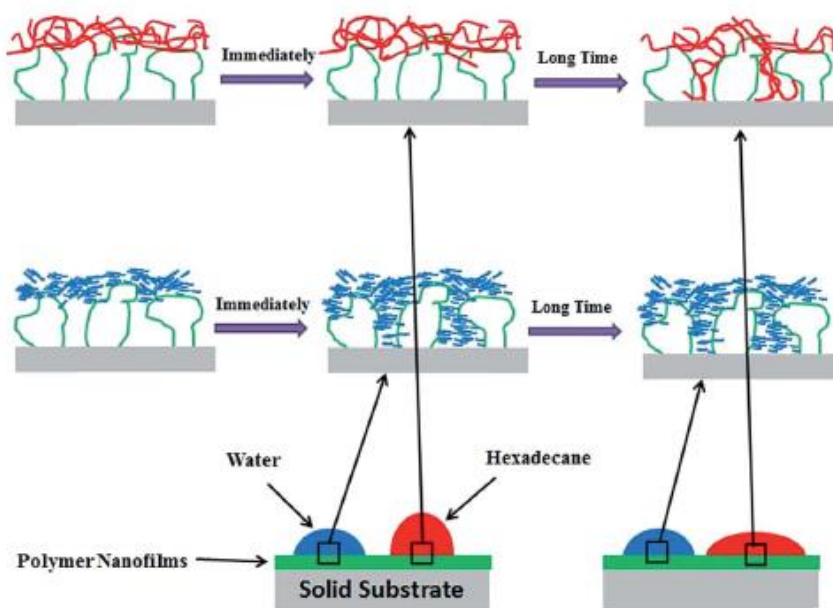


Figure 5: Schematic of penetration of ZDOL film by water and hexadecane. Reproduced from Ref 23 with permission of The Royal Society of Chemistry.

The behavior of Z-03 and Z-tetraol confirm this hypothesis. Z-03 lacks a hydroxyl group, so its bond to silica is weaker than ZDOL. This leads to a less orderly film, one that leads to a higher WCA than HCA. Z-tetraol has extra hydroxyl groups, so its bond is even stronger than ZDOL. This very orderly film leads to a high WCA and HCA, as neither molecule can penetrate the film. For both Z-03 and Z-tetraol a time dependent HCA chart shows a flat line. The last piece of evidence needed was to replace silica with poly(tetrafluoroethylene) (PTFE). ZDOL cannot bind effectively with PTFE, so the film should have been less packed leading to a high WCA and low HCA. This was the case; in fact, the WCA and HCA values were similar to

those of uncoated PTFE, strongly suggesting that both water and hexadecane penetrate through the polymer film. The last item of note was the change in the rate of HCA decrease with respect to ZDOL film thickness. Using a modified Kohlrausch-Williams-Watts (KWW) function the $\cos \theta$ vs time plots of ZDOL were fitted. It was found that the rate of change for the thicker film (1.8 nm) was forty times slower than the rate of change for the thinner film (0.9 nm). This correlates with the penetration theory; it should take longer for liquids to penetrate a thicker film ²³.

3.0 METHODOLOGY

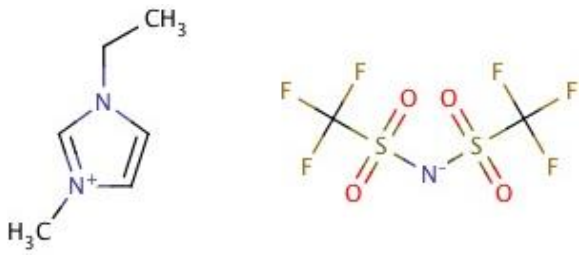
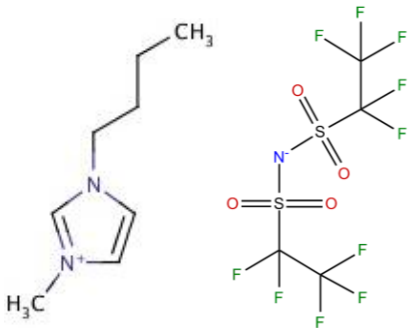
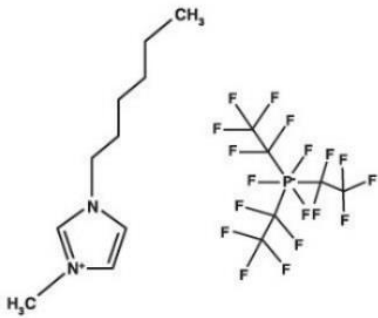
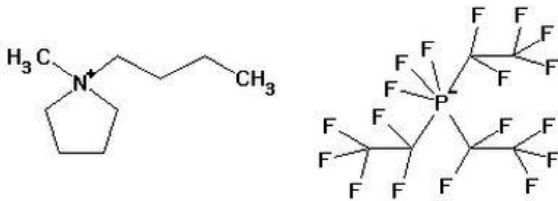
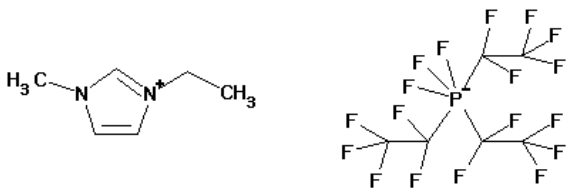
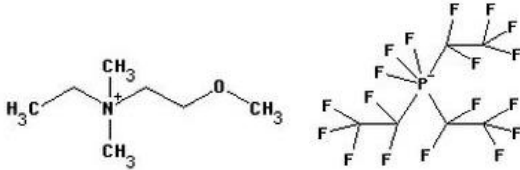
3.1 MATERIALS

A list of ionic liquids used, where they were purchased from, and their properties are assembled in Table 1. Their chemical structures are shown in Table 2. All ionic liquids were used as received. 2,3-Dihydrodecafluoropentane (Dupont VERTREL XF) was used as a solvent. SiO₂ wafers with native oxide (P/B <1 0 0> 1-10 OHM-CM 279±25 µm) were purchased from Silicon Quest International Inc; these were used as substrate.

Table 1: Properties and Vendors of Ionic Liquids Utilized

Chemical Name	Vendor	MW (g/mol)	Density (g/cm ³)
Shorthand Name			
1-ethyl-3-methyl-imidazolium bis(trifluoromethylsulfonyl)imide	Covalent Associates Inc.	391	1.51
EMIIm			
1-butyl-3-methyl-imidazolium bis(perfluoroethylsulfonyl)imide	Covalent Associates Inc.	NA	NA
BMIBeti			
1-hexyl-3-methyl-imidazolium tris(pentafluoroethyl)trifluorophosphate	Merck	612.29	1.56
HMZM			
1-butyl-1-methyl-pyrrolidinium tris(pentafluoroethyl)trifluorophosphate	Merck	587.27	1.59
BMPL			
1-ethyl-3-methyl-imidazolium tris(pentafluoroethyl)trifluorophosphate	EMD Chemical (Sub. of Merck)	556.17	1.71
EMZIA			
ethyl-dimethyl-(2-methoxyethyl) ammonium tris(pentafluoroethyl)trifluorophosphate	EMD Chemical (Sub. of Merck)	577.23	NA
MOEDEA			

Table 2: Chemical Structures of Ionic Liquids Utilized

	
<p>1-ethyl-3-methyl-imidazolium bis(trifluoromethylsulfonyl)imide</p>	<p>1-butyl-3-methyl-imidazolium bis(perfluoroethylsulfonyl)imide</p>
<p>EMIm</p>	<p>BMIBeti</p>
	
<p>1-hexyl-3-methyl-imidazolium tris(pentafluoroethyl)trifluorophosphate</p>	<p>1-butyl-1-methyl-pyrrolidinium tris(pentafluoroethyl)trifluorophosphate</p>
<p>HMZM</p>	<p>BMPL</p>
	
<p>1-ethyl-3-methyl-imidazolium tris(pentafluoroethyl)trifluorophosphate</p>	<p>ethyl-dimethyl-(2-methoxyethyl) ammonium tris(pentafluoroethyl)trifluorophosphate</p>
<p>EMZIA</p>	<p>MOEDEA</p>

3.2 EXPERIMENTAL PROCEDURE

A solution of ionic liquid in VERTREL was prepared, either from pure IL or diluted from a pre-made solution. The substrate, silicon wafer, was cleaned with a UV/O₃ cleaner for 15 minutes, then clamped to a dip coater; if film thickness was to be measured, after cleaning the oxide layer thickness was measured via ellipsometry, and set constant in the thickness model. The substrate was dipped into a plastic pitcher with minimum 100 mL solution, at a rate of 60 mm/sec with about 30 seconds of dwell time. Then the sample was measured for film thickness, observed in an optical microscope, and analyzed in AFM. Samples were also subject to contact angle testing and ARXPS analysis.

3.3 UV/O₃ CLEANING

The UV/Ozone Cleaner (ProCleaner 110, BioForce Nanosciences, Inc.) was used to clean the bare silicon wafer prior to coating. The instrument is shown in Figure 6. The cleaner works by emitting two wavelengths of radiation from a low-pressure mercury discharge tube. The smaller wavelength, 184.9 nm, causes molecular oxygen to dissociate into ozone and atomic oxygen. The larger wavelength, 253.7 nm, causes hydrocarbons to dissociate. The fragments are susceptible to reduction by the atomic oxygen. The products of that redox reaction are volatile compounds like CO₂, H₂O, and N₂. Finally, the high absorption of O₃ is at a maximum at a radiation wavelength of 253.7 nm, which converts the O₃ back into molecular oxygen. As such emitting both wavelengths ensures the continuous formation of atomic oxygen and hydrocarbon fragments which react into volatile compounds that evaporate away from the surface ²⁴. This

ensures the silicon wafer surface is free of hydrocarbon containments. The silica wafers were treated for about 15 minutes to remove all hydrocarbon contaminants.



Figure 6: UV/Ozone ProCleaner

3.4 DIP COATER

Fabrication of the ionic liquid film on the silica wafer substrate was done by dip-coating. The dip-coater used was the KSV Instruments KSV-DCX2 Dip Coater (shown in Figure 7). The instrument was used on a Kinetic Systems vibration-free platform to minimize the effect of vibrations on dip coating. The withdraw rate was kept constant at 60 mm/min for all samples made. The dip coating procedure in this study is the same as described in a previous work of IL film on silica ¹⁷.



Figure 7: KSV-DCX2 Dip Coater

3.5 ELLIPSOMETRY

Film thickness was measured using an alpha-SE from J.A. Woollam Co. The instrument is shown in Figure 8. The set up includes a light beam that serves as a monochromatic light source, a polarizer that produces linearly polarized light, a compensator controlled by a computer, the sample stage, an analyzer with adjustable azimuth angle, and a detector that can measure amplitude and phase difference between two orthogonal electric field components of emergent light ²⁵.



Figure 8: alpha-SE Ellipsometer

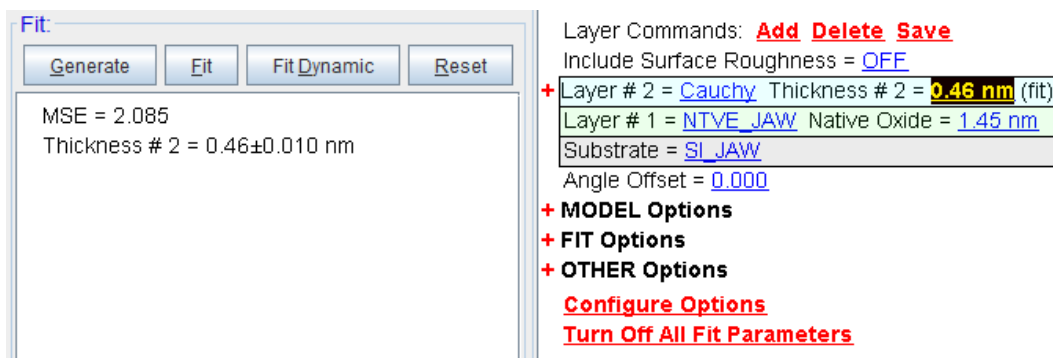
Ellipsometry works by measuring the change in amplitude and phase difference of polarized light after it is reflected from the sample. This change is dependent on the optical properties of the sample as well as the sample thickness. Because thickness is not independent of the optical properties and because these properties are dependent of the wavelength of the incident light, a dispersion relationship describing the optical constant shape is used for calculation. By adjusting the parameters of the dispersion model and the measured sample thickness, the amplitude ratio and phase difference can be calculated for an incidence light of known polarization. Thus by comparing the calculated values to the experimental values, the sample thickness can be measured ²⁶. The difference in these values is symbolized by the mean square error (MSE); the lower the MSE, the better the calculated data (and thus the measured sample thickness) aligns with the experimental data. For multi-layered samples, such as a silica wafer with thin film, coating separate models must be used for each layer; this way the thickness of each layer can be calculated. A two-layer model was used to determine the thickness of the IL thin film samples. First, a built-in Si-native oxide model was used to calculate the silicon oxide layer thickness. The oxide layer thickness was measured after UV cleaning and prior to dip-

coating. The average of three oxide layer measurements was set as the constant oxide layer thickness. Next, the Cauchy dispersion model was used to model the IL film. The Cauchy model is shown below:

$$n(\lambda) = A + \frac{B}{\lambda^2} + \frac{C}{\lambda^4}$$

The Cauchy model is used for many non-light-absorbing transparent materials; with only three parameters to adjust, it is simple to get an accurate optical constant shape. The Cauchy model has been used for IL thin films before ¹⁷. Parameter values A=1.45, B=0.0100, and C=0 were found to yield measurements with MSE values below 5.0. These parameter values were used for all IL thin film thickness measurements. An example of the use of the Cauchy model to calculate film thickness is shown in Figure 9.

a)



b)

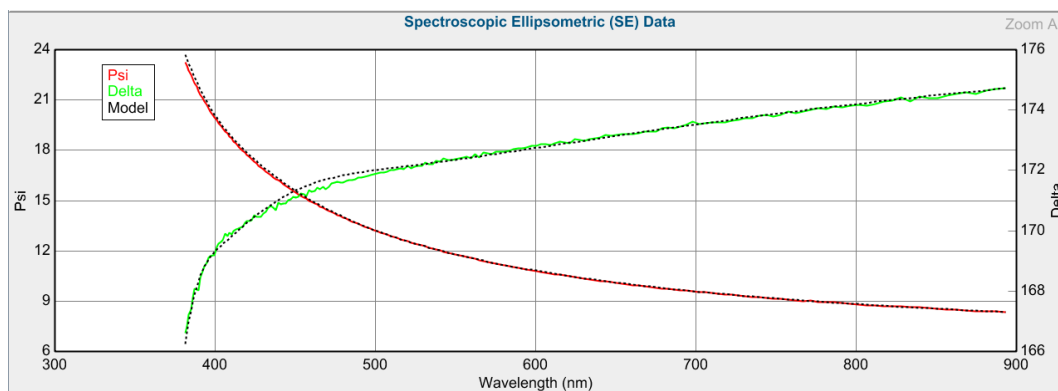


**Figure 9: a) Cauchy Model Parameter Interface;
b) Data fitting of amplitude ratio (Psi) and phase shift (Delta)**

3.6 GONIOMETER

Contact angle was measured using a VCA optima XE goniometer. The instrument is shown in Figure 10. For each measurement a droplet was dispensed (2.5 μL distilled water, 3.0 μL hexadecane) from a syringe; because the droplet clung to the tip, the goniometer stage was raised so that the sample made contact with the droplet. For static contact angle the image was taken immediately and the contact angle was measured via VCA software. For time-dependent trials the droplet and sample were left on the stage uncovered. A batch file was used to run

HyperCam, a screen capture video program, at certain time intervals. Frames were taken from the videos obtained and the VCA software was used to calculate the contact angle of the images from the frames. Advancing and receding contact angle were obtained by first dispensing a droplet onto the sample, then lowering the needle to the droplet. VCA software was used to record video of liquid dispensing or withdrawal and calculate the contact angle from frames from the video. The advancing and receding contact angle was measured at the frame right before a visible movement shift in the droplet. To verify that the angle measured was the true advancing or receding angle a graph was constructed of the contact angle of the droplet over the course of the time of the video; the advancing contact angle would be the maximum contact angle for an expanding droplet while the receding contact angle would be the minimum for a receding droplet.



Figure 10: VCA optima XE Goniometer

3.7 OPTICAL MICROSCOPY

Samples were analyzed using a Zeiss Axio Lab optical microscope. The instrument is shown in Figure 11. The AxioVision Rel. 4.8 software allowed for real-time image processing on computer. The microscope was first set to the lowest magnification. The stage was adjusted until it was confirmed that the focus was on the sample. After a point of interest was selected the magnification was increased to the desired value; the resulting image was saved via the AxioVision software, corrected for color, and length scale was added based on the magnification used.



Figure 11: Zeiss Axio Lab Optical Microscope

3.8 ATOMIC FORCE MICROSCOPY

Samples were analyzed using the Veeco Manifold Multimode V- Dimension V Combination Scanning Probe Microscope (shown in Figure 12). NanoScope v720 software was used to operate the AFM and analyze the image results. Tapping Mode AFM was used to analyze the samples. Tapping mode AFM works via a feedback system that measures the change in the oscillation of a cantilever that occurs due to intermolecular forces between the atomically precise cantilever tip and the sample surface. A voltage is applied to a piezo-vibrator to drive cantilever oscillations at a set amplitude and frequency. As the cantilever tip comes into contact with the sample surface attractive and repulsive forces will cause a change in the amplitude as well as a phase shift. By measuring the change in voltage required to maintain the amplitude at the setpoint, the topography of the sample can be mapped out ²⁷. The sensitivity factor that connects the change in the voltage to the change in topography Δz is connected to the force applied to the cantilever. The expected tip-sample forces can be estimated by a rough calculation of the forces between atoms in a solid ²⁷. The forces come out to be in the nanonewton range. As such the forces between the tip and the sample should be within this range to avoid disrupting the bonds of the surface atoms. By keeping the cantilever spring constant low (within 10 N/m, about the same spring constant for a harmonic oscillation model of two atoms) the deflection measurement will be in the angstrom range ²⁷. As such it is not unusual for AFM measurements to be in the nanometer range, especially when cantilevers of low spring constants are used. Tapping mode is also known as semi-contact mode because cantilever tip only comes into contact with the sample surface on the lower semioscillation of the cantilever. This minimizes the amount of contact the tip has with the sample without loss of topography data. Tapping mode is useful when scanning

sensitive samples such as thin film samples. Tapping mode AFM has been used to characterize IL thin film topography before with no reports of damage to the film surface ¹⁷.

Cantilevers purchased from MikroMasch were used. Two types of probes were used: a stiff probe (325 kHz, 40 N/m) and a soft probe (160 kHz, 5.0 N/m). In addition to topography imaging, section and roughness analysis were used to characterize the samples.

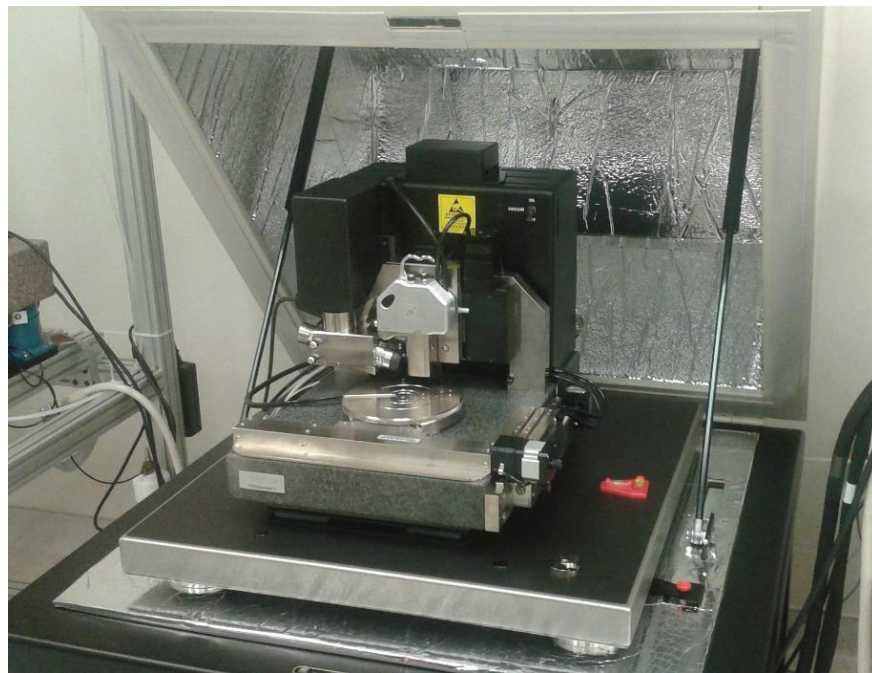


Figure 12: Veeco Manifold Multimode V- Dimension V Combination SPM

3.9 X-RAY PHOTOELECTRON SPECTROSCOPY (XPS)

Samples were analyzed using the Thermo Scientific ESCALAB 250Xi X-Ray Photoelectron Spectroscopy System. The sample is bombarded with Al $k\text{-}\alpha$ x-rays with a known energy (1486.7 eV). The energy of the x-ray photons is passed to the electrons in the sample molecules upon contact, causing some of them to be ejected. The ejected electrons will have a kinetic energy relative to how bound they are to the atoms in the molecule; the higher the binding energy (i.e., the more tightly the electrons were bound to the atom), the lower the kinetic energy of the ejected electrons will be. The binding energy is dependent on several factors, including the atom element and the electron configuration state, both standard orbitals and hybrid orbitals. The ejected electrons are picked up by an electron detector. The detector can record the kinetic energy of these electrons as well as the number of electrons with a specific kinetic energy. Thus by calculating an energy balance of the energy of the photons and the kinetic energy of the electrons detected (corrected for energy loss as the electrons strike the sample), the various binding energies present in the sample can be obtained. The resulting data output is a graph of electron count and binding energy. By analyzing the peaks of electron count at specific binding energies, the presence of certain elements and compounds can be confirmed; further analysis of the area under the peaks can reveal the ratio of compounds present, reported as atomic percent ²⁸. The quality of the spectra generated depends on the energy filter and the operating mode. The most common energy filter in use in modern XPS is the concentric hemispherical analyzer (CHA); up to 0.01 eV energy resolution is possible with the CHA, and the kinetic energy values obtained have less a dependence on the distance between the filter and the sample. The most common operating mode used in XPS operation is constant analyzer energy/fixed analyzer transmission mode (CAE/FAT). In CAE/FAT the electrons are accelerated or decelerated to a

constant energy value before entering the filter. This value is referred to as the pass energy. By lowering the pass energy, the resolution is increased, albeit at the cost of the sensitivity. A scan conducted with monochromatic Al- $\text{K}\alpha$ source with a CHA filter at a pass energy of ~ 5 eV is capable of a resolution up to 0.4 eV²⁸. An initial survey scan is conducted first to get a general idea of the elements and bonds present in the sample. After that, a high-resolution scan focusing on a specific binding energy range is conducted for a more detailed analysis of specific elements or bonds. For imidazolium-based ionic liquid samples, high-resolution scans of nitrogen are conducted; the two nitrogens on the imidazolium cation yield a large distinct data peak that is easy to compare to other nitrogen peaks present.

Analyzing the data involves calculating the atomic percentage of all the elements and bonds present as indicated by the binding energies recorded. By noting the binding energy values where there are spikes in the electron count (data peaks) and normalizing the areas under all of the peaks in the spectrum, the relative amount of each element and/or bonds can be obtained, and thus, the ratio of different compounds that make up the sample. This can be used to determine if molecular ordering is occurring. By comparing the ratio of atomic percentages (the atomic ratio) to the stoichiometric ratio, it is possible to determine if one of the molecules is layered over the others by seeing how the two ratios differ; the closer the atomic ratio is to the stoichiometric ratio the more random the molecular arrangement is. Further confirmation can be obtained from angle-resolved XPS scans (ARXPS). ARXPS works just like regular XPS, except now the sample stage can be tilted to change the angle at which the photons strike the sample (known as the takeoff angle). The reason for doing this is to analyze the sample at different depths. At a 0° (flat sample), the photons can strike molecules both at the surface and in the bulk, so the emitted electrons come from almost all of the molecules in the sample. Increasing

the takeoff angle, especially for a thin film sample, ensures that the photons will only strike the molecules on the surface, so now the electrons will come only from those surface molecules ²⁸. By comparing the spectra obtained at different takeoff angles, it can be determined if there is molecular arrangement. If there is some sort of arrangement, then the atomic ratio should change as the angle changes; at a tilt, only the surface is scanned, so in effect, only one “layer” is seen as opposed to all “layers” (i.e., the bulk). If there is no arrangement, then the ratio should stay constant. A previous study of IL thin films did ARXPS scans of 0° and 60° takeoff angle and revealed a change in atomic ratio for certain samples ¹⁷. As such, the same settings were used in this study.

An initial survey scan was done at 1.00 eV, CAE 150.0, 200 μm , 5 scans. Then high-resolution scans were focused for N 1s peaks, set at 0.10 eV, CAE 50.0, 200 μm , 10 scans. The scan resolution for the N 1s spectra was 0.1 eV. Scans were done at 0° and 60° takeoff angle.

4.0 RESULTS AND DISCUSSION

4.1 TOPOGRAPHY OF EMIIIM THIN FILM

Ellipsometry was used to measure EMIIIm thin film thickness on a silicon wafer for different dip-coating solution concentrations. A graph of thin film thickness as a function of concentration is shown in Figure 13; raw data with MSE is shown in [Appendix A](#). As seen in Figure 13, there is a positive linear relationship between the solution concentration and the thin film thickness; as the solution concentration increased the thickness of the thin film formed by dip-coating increased. This trend is shown in Figure 13 via the black line of best fit. A positive linear relationship was seen before for DMPIIm thin film ¹⁷. The measurements obtained with the chosen Cauchy model constants were fairly consistent. Most of the thickness data obtained for each solution concentration had a standard deviation below 0.04 nm, with the exception of the 0.5 g/L data set and the 1.0 g/L data set. The MSE values were also low for almost all measurements, never exceeding 5.000 with one important exception; this means that for almost all of the samples, the chosen Cauchy model accurately calculated the film thickness. It is important to note that there is a small increase in the MSE for the 0.75 g/L and the 1.0 g/L samples. The MSE for the samples made from a lower solution concentration fluctuate between 1.5 to 3; the MSE for the second and third highest concentration were consistently in the 3-4 range. Then there is the MSE of the 5.0 g/L samples to consider. The MSE spikes to an average

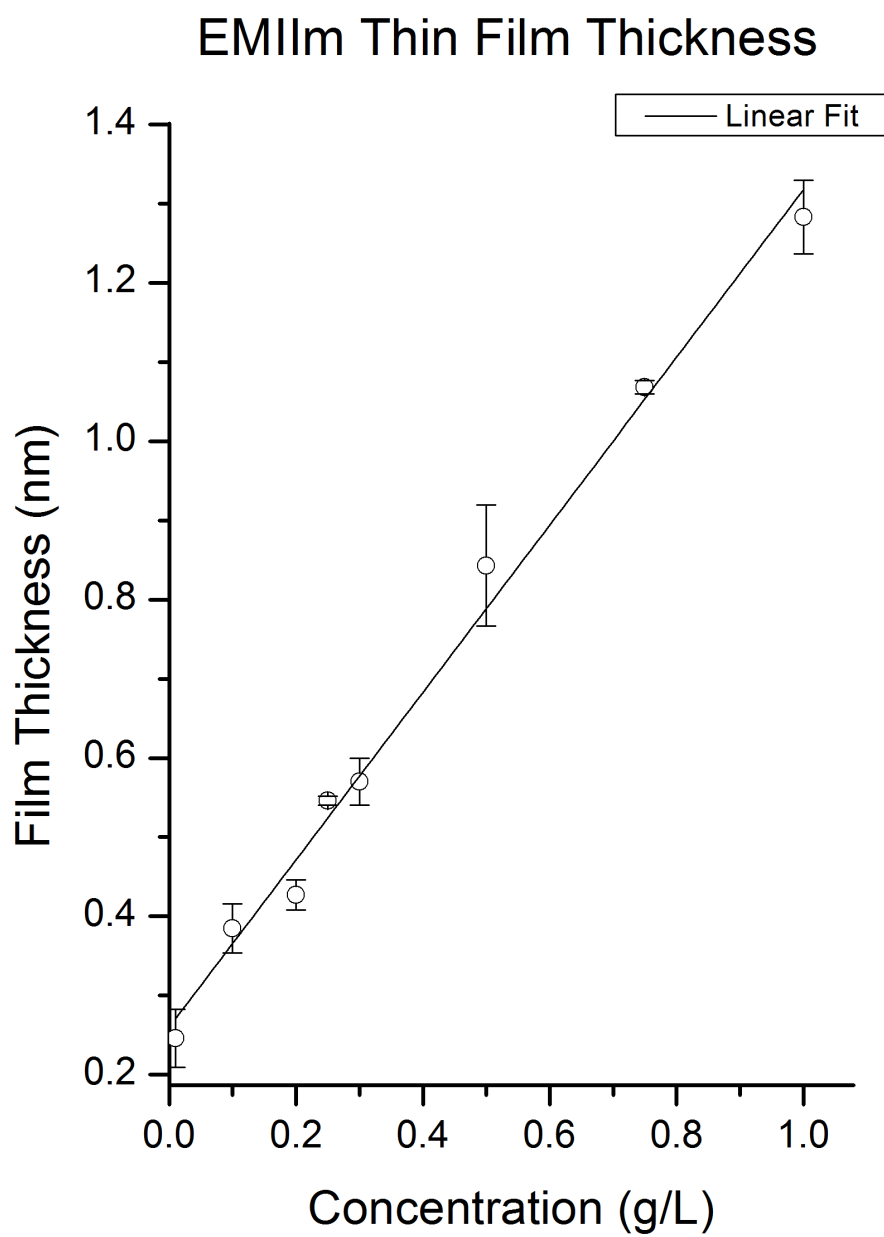


Figure 13: EMIIm film thickness vs. dip coating-solution concentration, with a linear trendline

of 26, indicating that the chosen Cauchy model is a poor fit. The slow rise in the MSE followed by that spike indicates that there is a shift in the optical properties of the IL thin film as the solution concentration/film thickness increases. A change in the optical properties must be due to a chemical or physical change in the IL thin film as the film thickness increases. Given the lack of any other chemical reagent present the change must be a physical one that occurs past a certain film thickness. A sound hypothesis then would be the development of dewetting on the film past a certain film thickness. As stated before, dewetting occurs when the surface tension of the ionic liquid exceeds the electrostatic interaction between the ions and the substrate. As the cations are drawn to the substrate they form a layer to maximize contact. This in turn causes a layer of anions to form and so on and so forth. However, the main driving force for this layer formation is still the initial charge of the substrate. As more layers form and the film grows thicker the influence of the substrate decrease. Hence at a certain point droplets begin to form on the film (i.e. film dewetting). Film dewetting would explain the gradual change in optical properties, if the droplets are sparse small relative to the film thickness. If the severity of the dewetting increases with film thickness, then there would be a point at which the optical properties would be radically different from that of thinner films. For EMIIIm thin film on silica that point appears to be around 3 nm, the film formed from a 5 g/L solution concentration.

For further analysis of the dewetting behavior, the monolayer thickness (ML) of EMIIIm was calculated. A monolayer is defined as one closed layer of vertically arranged ion pairs; a monolayer of ions completely covers the substrate with no gaps or unpaired ions. Monolayer thickness is calculated by converting molar volume to size per molecule, assuming cubic volume arrangement ¹⁷:

$$\hat{V} = \frac{M}{\rho}$$

$$\hat{V}_{molecule} = \frac{\frac{M}{6.02 * 10^{23}}}{\rho}$$

$$Cubic: \hat{V}_{molecule} = (s_{molecule})^3$$

$$s_{molecule} = (\hat{V}_{molecule})^{\frac{1}{3}}$$

The ML value for EMIIIm is 0.75 nm (i.e. 1 ML of EMIIIm = 0.75 nm). Thickness values will now be reported in “units” of ML, accurate to 0.1.

To verify whether dewetting is occurring, the film topography of three thin film samples of increasing thickness were analyzed via optical microscope and AFM. Figure 14 shows optical images of EMIIIm thin films of thicknesses 0.6, 1.1, and 1.7 ML (± 0.1 ML); all of the images were taken at the maximum magnification. For the 0.6 ML sample, the image shows a smooth surface with specks of what appears to be dust. The images of the 1.1 ML and 1.7 ML samples are similar with one important difference: small dark spots of even distribution around the surface.

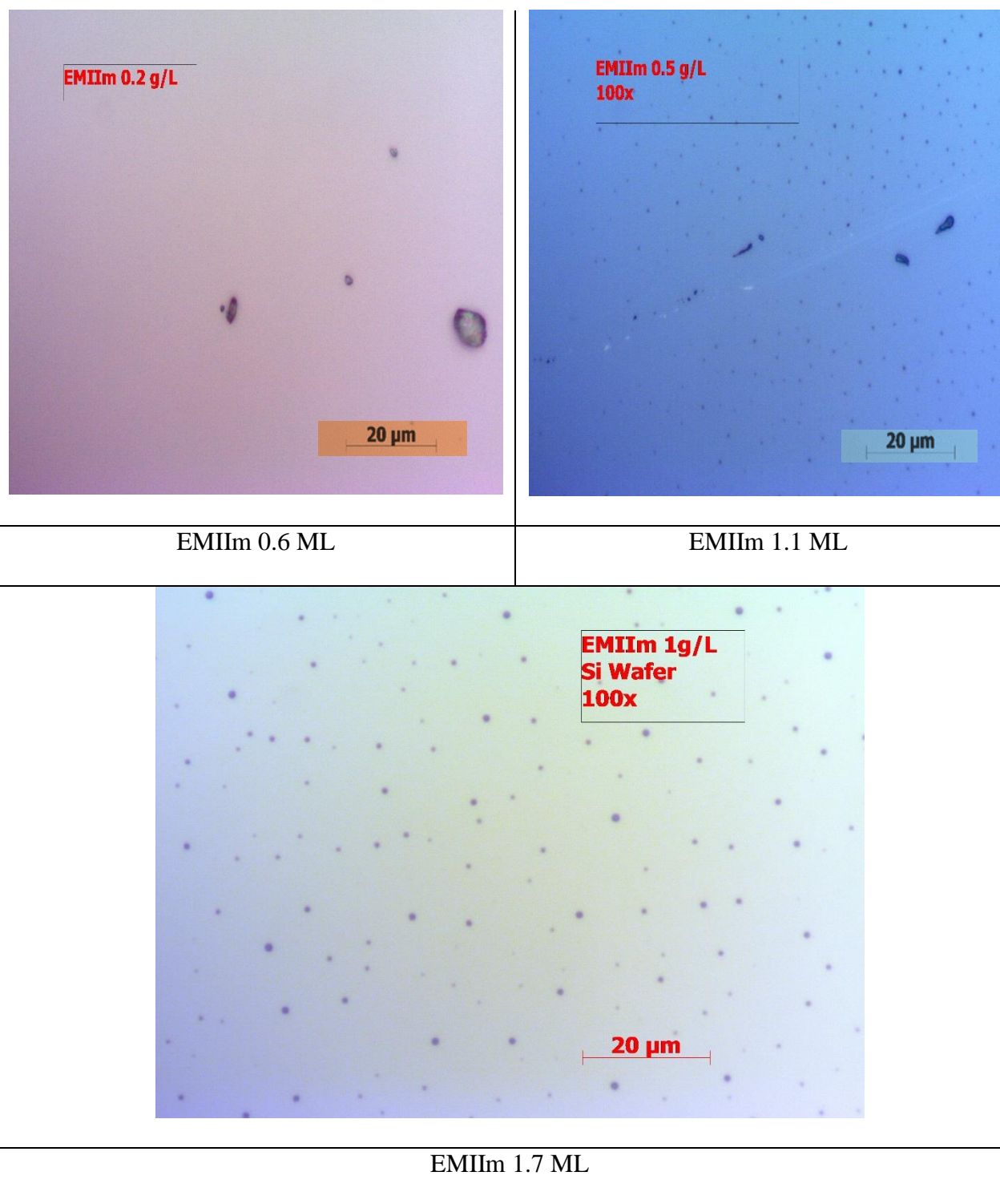


Figure 14: Optical images of EMIIm film on silica, of thickness 0.6, 1.1, and 1.7 ± 0.1 ML

The spots appear to be similar in size for both samples and appear different from the dust particles still present on both samples; the spots are smaller and more uniform in shape, while the supposed dust is larger and irregular in shape. AFM topography images of the same three samples are shown in Figure 15. The AFM image of the 0.6 ± 0.1 ML sample show a smooth even film with the odd dust particle, just like the optical images. The image of the 1.1 ± 0.1 ML sample shows a slightly irregular film with round spots of slightly higher height than the film. The 1.7 ± 0.1 ML sample image is similar, but now the spots are larger and seem to have a height change along the edges. So far this suggests that dewetting is occurring, and that dewetting increases in severity as the film thickness increases.

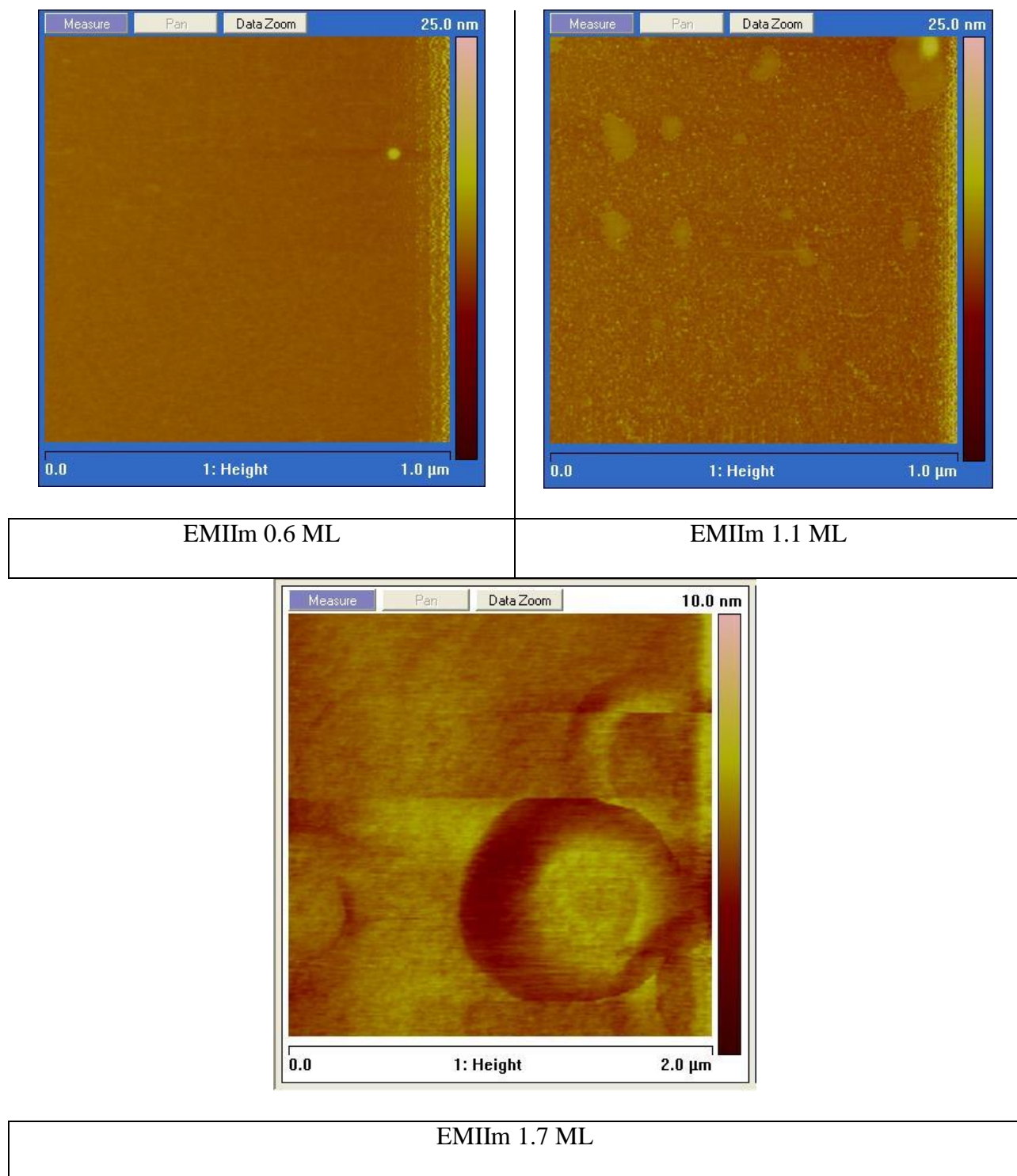
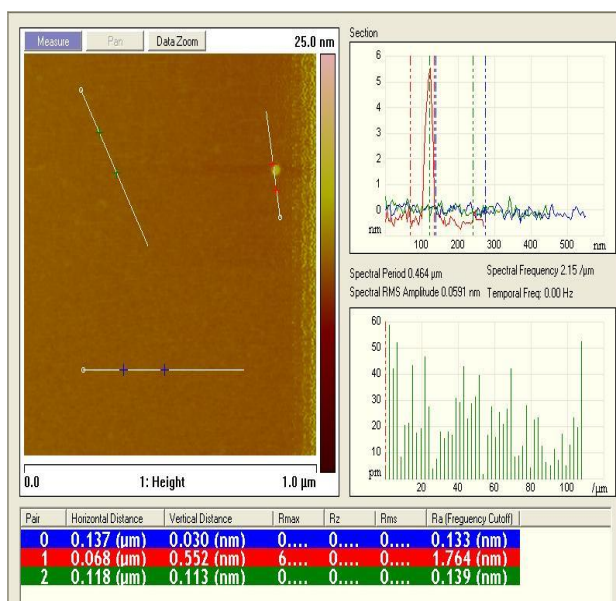
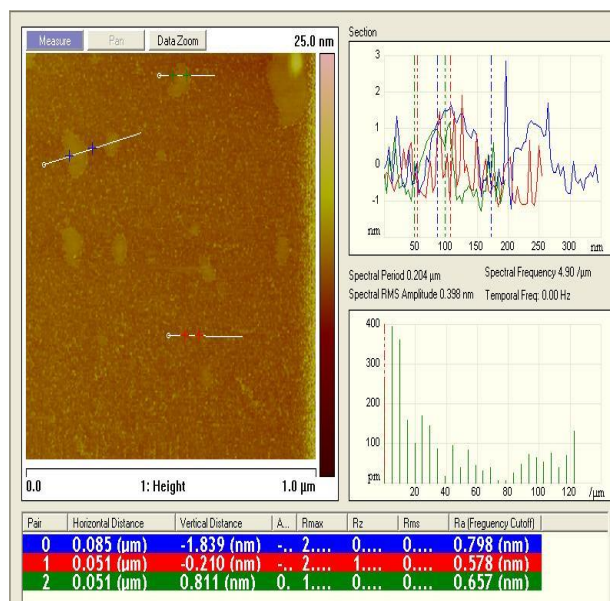


Figure 15: AFM topography images of EMIIIm film on silica, of thickness 0.6, 1.1, and 1.7 ± 0.1 ML

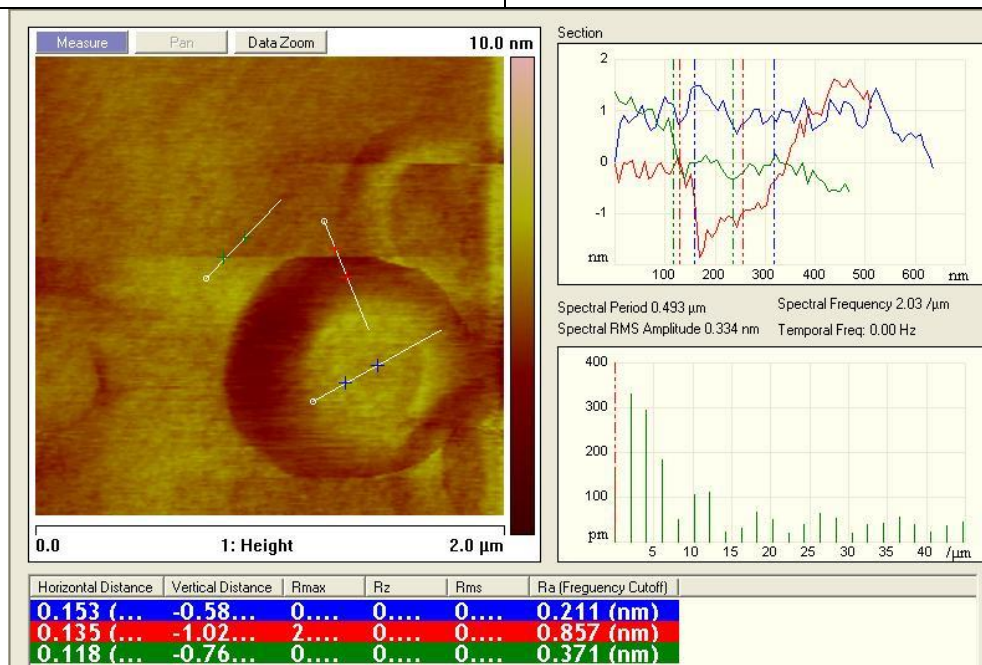
For further examination AFM section analysis was conducted for the three samples, seen in Figure 16. The cross section graph confirmed that the spots are indeed droplets. The height profiles along the spots on the 1.1 ± 0.1 ML and 1.7 ± 0.1 ML samples show a gradual rise from the film surface that plateaus at 1.0 ± 0.1 nm for ~ 0.1 μm (1.1 ML profile) or 1.5 μm (1.7 ML profile) (lengths accurate to 0.1 μm) before decreasing back to zero. However, a height profile along the spot on the 0.6 ± 0.1 ML sample showed a spike in the height (6.0 ± 0.1 nm) that barely lasts $0.0(3)$ μm . Given what was seen in the optical images it is safe to assume that the spot on the 0.6 ML sample is a dust particle, while the spots on the other samples are droplets. The second thing to note is the change in the cross section graph. For the 0.6 ML sample the cross section graph is centered around 0.0 nm height for two different section directions with little deviation. However, the graphs for the other two samples are much more chaotic, as the height varies greatly even in sections not including the droplets. This suggests that along with dewetting the film structure changes to a sponge-like structure, as seen before for DMPIIm¹⁷. This is further supported by the average roughness (Ra) values obtained in the section scans. For the 0.6 ML film the Ra values along the film are $0.1(3)$ and $0.1(4)$ nm, i.e. the mean value of the height from the surface plane along the two sections is $0.1(3)$ nm and $0.1(4)$ nm. For the 1.1 ML film the Ra values jump; along the droplets the Ra value is 0.7 ± 0.1 and 0.8 ± 0.1 nm, while along the film the Ra value is now 0.6 ± 0.1 nm. The increase in Ra corresponds to the chaotic changes in height seen in the section profile graphs, indicating a sponge-like structure over a smooth film. Finally, the 1.7 ML film saw a decrease in Ra along the sections. Along the droplet edge the Ra value was 0.9 ± 0.1 nm, corresponding to the sharp decrease in height. On top of the droplet the Ra is 0.4 ± 0.1 nm; this is similar to the Ra of a section along the film surface, 0.2 ± 0.1 nm.



EMIIm 0.6 ML



EMIIm 1.1 ML



EMIIm 1.7 ML

Figure 16: AFM section analysis of EMIIm film on silica, of thickness 0.6, 1.1, and 1.7 ± 0.1 ML

While the R_a values may suggest that the film is now broken into patches of smooth film and bare substrate, the vertical distance of the sections disprove this. The “patches” are still sponge-like, as the vertical distance along the top of the droplet is -0.6 ± 0.1 nm in contrast the vertical distance of 0.1 ± 0.1 nm for the 0.6 ML smooth film. In addition, the vertical distance along the droplet edge (-1.0 ± 0.1 nm) remains below the thickness measured via ellipsometry (1.3 ± 0.1 nm). A formal roughness analysis was done for the three film samples as well as bare silica for use as a control. The results for a $5.0 \mu\text{m}$ scan size for each sample is shown in Table 3; the values used are the image values i.e. the roughness of the entire scan. As it can be seen for the three film samples tested there appears to be complete coverage; the roughness values for the samples are very different compared to bare silica. The similarity of the R_a and R_q (root mean square height deviation) values between the bare silica and 1.7 ML samples seems to suggest that there is partial substrate exposure. However, the R_{max} value is still markedly lower, indicating there is still a layer covering the substrate below. As seen in the section analysis as the film thickness increases from 0.6 to 1.1 ML, the R_a value increases.

Table 3: Roughness analysis for bare silica and EMIIIm thin film

Thickness (± 0.1 ML)	NA (Bare Si)	0.6	1.1	1.7
R_a (± 0.1 nm)	0.6	0.1	1.1	0.6
R_q (± 0.1 nm)	0.8	0.3	1.8	0.9
Z Range (± 0.1 nm)	8.2	6.3	13.5	3.0
R_{max} (± 0.1 nm)	8.2	6.3	34.8	3.0

It should be noted that optical and AFM analysis was done for two other IL thin films. See [Appendix B](#) for a comparison of the topography of MOEDEA, EMZIA, and EMIIIm.

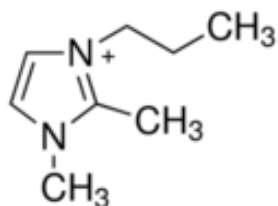
Two more observations can be made regarding the monolayer thickness and the AFM results. The first one concerns the 0.6 ± 0.1 ML sample. Normally this means incomplete coverage; this could be seen as bare substrate with patches of IL film, or a substrate covered by a checkerboard pattern of cations and anions. As proven by the roughness analysis, the substrate is indeed fully coated by the ionic liquid at 0.6 ML. It would seem that the ions prefer a horizontal arrangement, to be as close to the substrate as possible. However, silica is weakly negative, so the anions should not be able to be directly on the substrate. In other words, if there is incomplete coverage then there should be patches of IL film, as the anion would prefer to be on top of the cations. The only explanation would be that the monolayer is actually thinner than the calculated value. The monolayer thickness calculation assumes a cubic volume. If the ions can be densely packed then the volume would be rectangular, not cubic. This would permit full coverage without having anions on the surface. This would also confirm the second observation, the critical thickness of 1.1 ± 0.1 ML. By definition this means that as soon as the silica substrate is fully coated droplets begin to form on the film. Hence there needs to be an initial layer of ions present before dewetting first occurs. To confirm this the molecular arrangement of the thin film needs to be analyzed.

4.2 MOLECULAR ARRANGEMENT OF EMIIIm THIN FILM

To uncover the molecular arrangement of the EMIIIm thin films, ARXPS scans were taken of 0.6, 1.1, and 1.7 ± 0.1 ML film samples. A previous work with 1,2-dimethyl-3-propyl-imidazolium bis(trifluoromethylsulfonyl)imide (DMPIIm) thin film¹⁷ utilized high-resolution scans of nitrogen to get the atomic ratio of N^- and N^+ , the ratio of the imide nitrogen and the imidazolium nitrogens; this was used to determine the arrangement of the cations and anions in the film bulk and the film surface. It was decided that a similar scan could be done for EMIIIm thin film, since the two ionic liquids are very similar in structure (see Figure 17).

a)

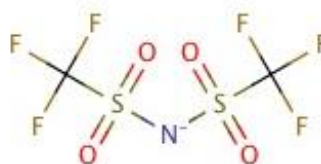
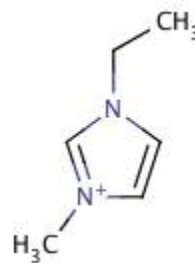
DMPIIm



ML = ~0.78 nm

b)

EMIIIm



ML = 0.75 nm

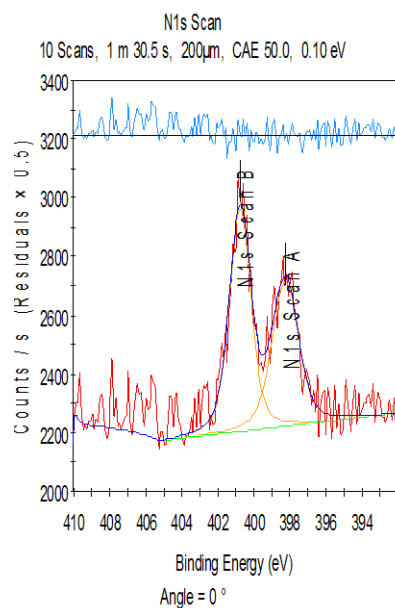
Figure 17: a) Structure, monolayer thickness of DMPIIm¹⁷; b) Structure, monolayer thickness of EMIIIm

The N 1s high-resolution spectra are shown in Figure 18. The peaks at $398-399 \pm 0.1$ eV and $400-401 \pm 0.1$ eV are assigned to N^- and N^+ respectively. The values obtained from curve-fitting the spectra are shown in Table 4. The atomic percent values used in calculating the atomic ratio were reported to 0.01 %, hence the atomic ratios of N^-/N^+ are reported to the same accuracy.

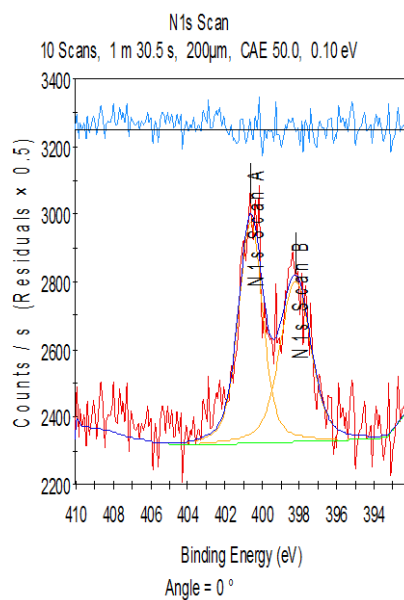
Table 4: ARXPS spectra (N 1s) fitting calculations for EMIm thin film

0° Takeoff Angle			
Thickness (± 0.1 ML)	0.6	1.1	1.7
Atomic Percent N^- (± 0.01)	44.42	41.73	41.23
Atomic Percent N^+ (± 0.01)	55.58	58.27	58.77
Atomic Ratio N^-/N^+ (± 0.01)	0.80	0.72	0.70
60° Takeoff Angle			
Thickness (± 0.1 ML)	0.6	1.1	1.7
Atomic Percent N^- (± 0.01)	48.53	41.47	43.48
Atomic Percent N^+ (± 0.01)	51.47	58.53	56.52
Atomic Ratio N^-/N^+ (± 0.01)	0.94	0.71	0.77

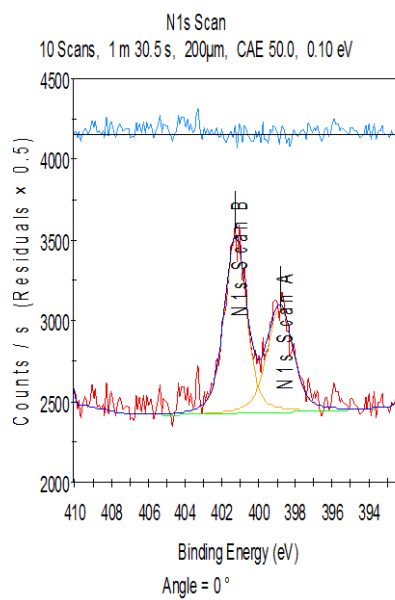
0.6 ML
0°



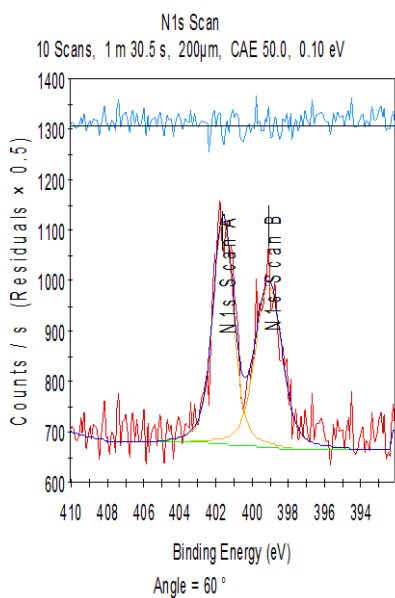
1.1 ML
0°



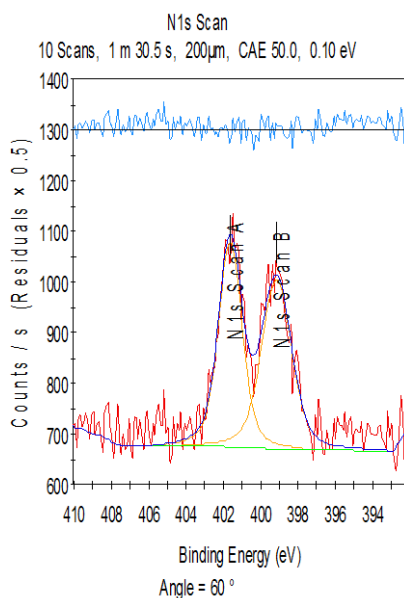
1.7 ML
0°



0.6 ML
60°



1.1 ML
60°



1.7 ML
60°

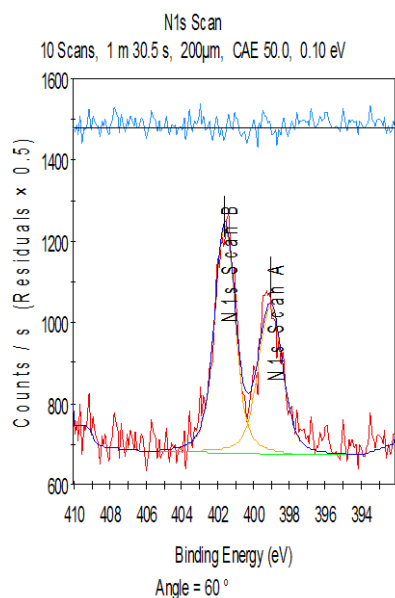


Figure 18: ARXPS spectra (N 1s) of EMIIIm thin film of thickness 0.6, 1.1, and 1.7 ML, at 0° and 60° takeoff angle

For the 0.6 ± 0.1 ML sample, N^-/N^+ ratio is 0.80 ± 0.01 at 0° emission angle, which indicates strong attenuation of anion over cation. In other words, this means that EMIIIm exhibits anion/cation layering. This conclusion is further supported by the fact that N^-/N^+ ratio of the same sample increases to 0.94 ± 0.01 at 60° emission angle; indicating that the surface is composed of an anion layer. On the other hand, for both the 1.1 ± 0.1 and 1.7 ± 0.1 ML sample spectra the N^-/N^+ ratio decrease to ~ 0.7 , and there is no dependence of N^-/N^+ ratio on the emission angle. The results here suggest that the thicker EMIIIm samples have a more randomized order of cation and anion, which is consistent with the dewetting seen in the AFM and optical microscopy images. This does not explain why the atomic ratio is greater than the stoichiometric ratio of 0.5 even for bulk arrangement. For that it is useful to compare the EMIIIm results to the study of DMPIIm thin film on silica. For DMPIIm the samples free of dewetting showed a change in N^-/N^+ ratio as the emission angle increased, whereas the dewetted samples showed no change. However, the bulk ratio was around 0.5, close to the stoichiometric ratio. The difference is due to slight structural difference between the cations of the ionic liquids. A study done by Rollins, Fitchett, and Conboy found that changing the alkyl chain length on an imidazolium cation changed the orientation of the cation on the silicon surface²⁹. Regardless of the alkyl chain length the cation would be the first layer closest to the silicon surface due to its weak negative charge. However, as the chain length decreased the cation would be oriented more parallel to the substrate. This is due to steric effects in film formation. Longer chains provide increased rotational freedom for the structure. This favors random bulk assembly over layer formation as it is less likely that the cation will be in a planar configuration. As seen in Figure 17 DMPI has a longer alkyl chain and an extra methyl group, giving the cation more rotational freedom which means it is less likely to be in a planar configuration. Overall this

means that a random bulk arrangement is favored over planar layers. This is seen in ARXPS as an atomic ratio close to the stoichiometric ratio, 0.5. On the other hand, EMI has a shorter chain and lacks one methyl group. With less rotational freedom the cation is more likely to be in a planar configuration. This means that layering is favored over bulk arrangement. This is why the atomic ratio is so much higher for EMIIIm, even for bulk scans and dewetted surface scans. Even a so called bulk arrangement will be semi-layered since EMI is more likely to be in a planar configuration, leading to more pockets of anions resting on top of the flat cations. Hence for EMIIIm the bulk ratio is 0.7, as there is a slightly greater presence of anions on the surface due to semi-layering.

This molecular arrangement is further confirmed by comparing the dewetting behavior of EMIIIm and DMPIIm. For DMPIIm dewetting was first seen at ~ 0.9 ML¹⁷. For EMIIIm dewetting is first seen at 1.1 ML. Moreover, it was confirmed that the monolayer thickness is actually lower than the calculate value, as this would allow for the complete film coverage observed in AFM analysis. Using the Rollins study it can be assumed that as the cation alkyl side chain length increases, the critical ML value for an ionic liquid on silicon decreases; dewetting will be seen at smaller film thickness because the IL will prefer to be in the bulk structure over layer structure. This is what is currently seen with DMPIIm and EMIIIm. Again, the lack of a methyl group and the smaller alkyl chain means that the EMI cation can layer better on the silica substrate than DMPI cation. This results in a stronger silica-cation attraction, which means dewetting occurs at a larger thickness. This also confirms that EMIIIm can pack better along the substrate, which explains why there is full coverage of the substrate even at 0.6 ± 0.1 ML.

In summary it was found that for EMIIIm film on silicon wafer an initial smooth film is formed with a layered arrangement of cations and anions. The imidazolium cation is closer to the weakly negative silica substrate while the trifluoromethylsulfonyl anion is closer to the surface. From at least 0.6 ± 0.1 ML full film coverage is observed, as seen by the drastic difference in roughness compared to bare silica. There is a critical dewetting ML value i.e. critical film thickness, at which the film will start to show signs of dewetting. For EMIIIm this critical thickness appears to be 1.1 ± 0.1 ML. In addition, at this thickness the film changes from smooth to rough, possibly sponge-like as observed with other IL films on silica¹⁷. However, AFM section analysis shows that the substrates remains fully covered. The dewetting and film roughness increases in magnitude as the film thickness increases past the critical value, though the droplets have not been observed to be of height greater than 1 nm, and the substrate remains fully coated. This is visualized in Figure 19.

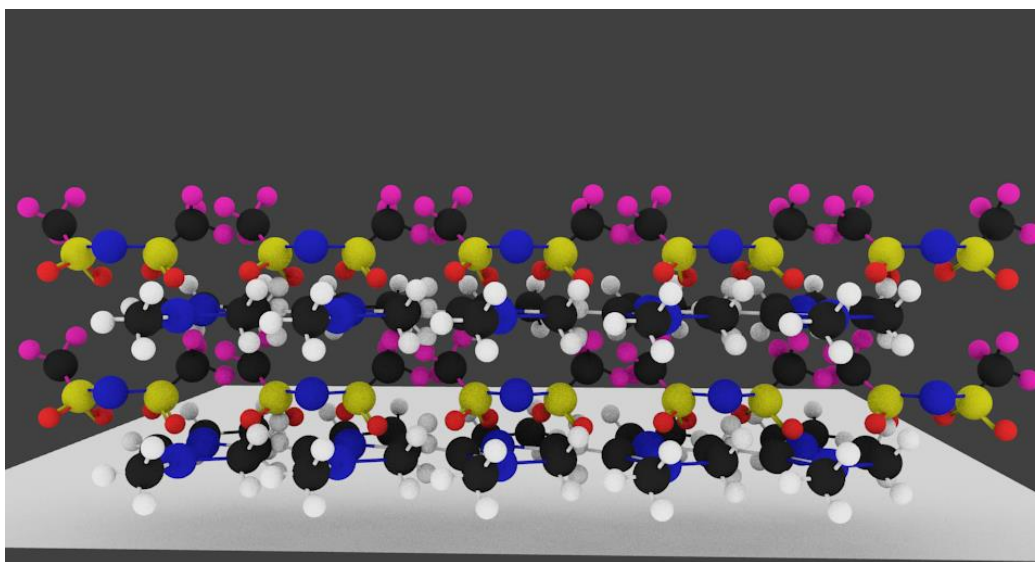


Figure 19: EMIIIm layered structure. The anion (yellow sulfur, pink fluoride) is near the film surface, while the cation (black carbon) forms the initial layer.

4.3 WETTABILITY OF EMIIM THIN FILM

Static contact angle data for various ionic liquid films are shown in Figure 20. A minimum of three measurements were taken for each ionic liquid film; each measurement was done on the same film sample. Each contact angle measurement consisted of a left and right angle measurement. The measurements were accurate to 0.01° . The average and standard deviation were calculated using both left and right angle measurements (i.e. six angle values were used, not three). The error bars shown in Figure 20 are the standard deviation of the data point. As it can be seen, for all ionic liquid films the WCA is lower than the HCA. Moreover, the WCA was consistently low, on average $10.37^\circ \pm 4.03$; for practical purposes all IL films tested were completely wetted by water. For the IL thin films tested, the high HCA can be partially explained by the fluorinated anions. All the ionic liquids tested featured anions with heavily fluorinated side chains (see Table 2). Even if some of the IL films tested exhibit dewetting, the presence of the fluorinated anions will repel hexadecane, resulting in a high static HCA. It is important to note that there is significant variation in the HCA among the different IL thin films tested. There is an 18.88° difference between the lowest HCA (BMPL 1.0 g/L) and the highest HCA (BMIBeti 5.0 g/L). However, there is only a difference in the HCA among different IL thin films. For two film of the same IL but made from different solution concentration the HCA is almost identical. The contact angle measurements seem to be reliable, as seen by the values obtained for bare silica and bare PTFE. The values obtained are close to contact angles obtained in past work ²⁰.

Static Contact Angles

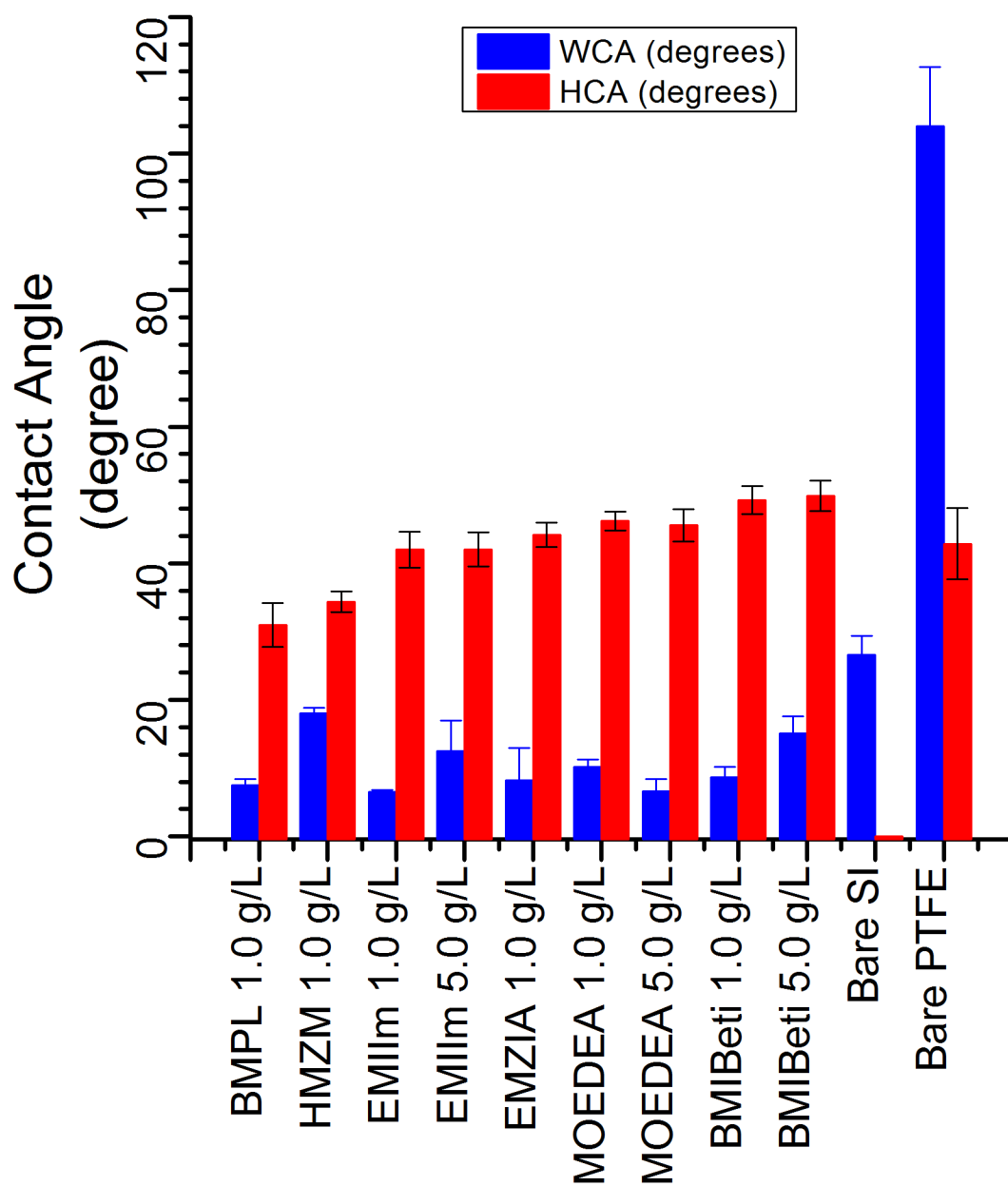


Figure 20: Static contact angle data with standard deviation for various ionic liquid thin films

In summary all IL thin films on silica substrate exhibited simultaneous hydrophilicity/oleophobicity. The WCA was consistently low, to the point of complete wetting for all films. However, the HCA varied for different ionic liquids, but for different solution concentration. The only commonality among the different ILs used is the fluorinated branches present in the anions. This only explains the high HCA; fluorinated branches can repel oils like hexadecane, as seen in other oleophobic coatings ¹². For more answers it is important to test an IL thin film with known topography.

To further explore the simultaneous hydrophilicity/oleophobicity the static contact angle for EMIIIm thin film on silica was measured for various film thicknesses. Figure 21 shows static contact angle for EMIIIm films of different thickness values. A minimum of five measurements were taken for each film thickness; not all measurements were done on the same film sample. Each contact angle measurement consisted of a left and right angle measurement. The measurements were accurate to 0.01 °. The average and standard deviation were calculated using both left and right angle measurements (i.e. ten angle values were used, not five). The error bars shown in Figure 21 are the standard deviation of the data point.

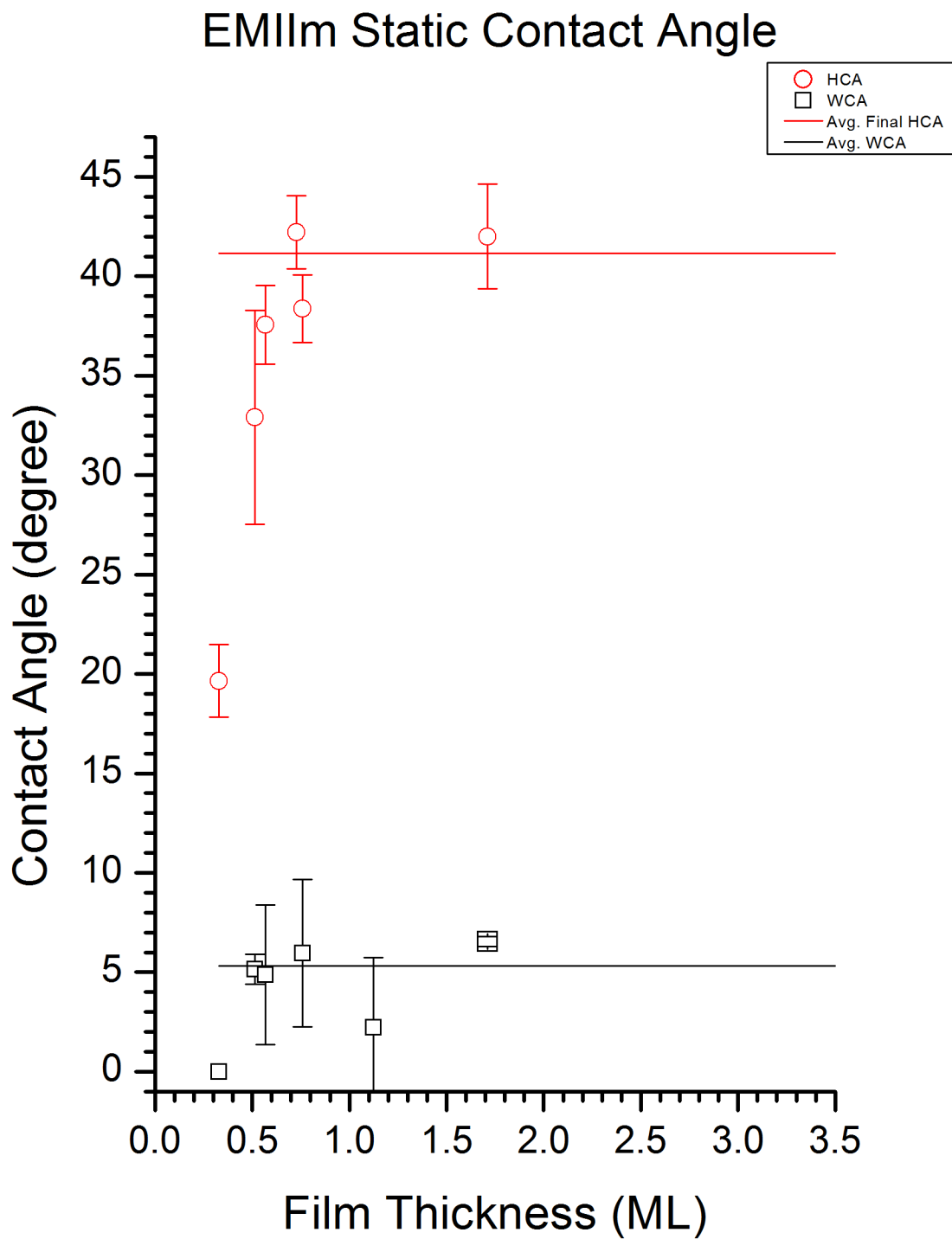


Figure 21: Static WCA and HCA for EMIIm thin film with standard deviation, WCA average line, and HCA plateau line

The first thing to note is is the plateau of HCA. The HCA increases until 0.7 ML thickness, at which point the HCA stays constant at $41.00^\circ \pm 0.01^\circ$ (shown in Figure 21 as the red line). The fact that the HCA plateaus below the critical thickness seems to suggest that surface topography does not play a role in the static HCA. Even for three different samples with dewetting the HCA remains roughly constant. The second point of interest is the rate at which the plateau is reached. The HCA only increases for about 0.3 ML before leveling off, increasing from 19.65° to 41.15° . This can be partially explained by examining the meaning of the monolayer thickness value. As proven in the previous section at 0.6 ± 0.1 ML the substrate is fully covered by the IL thin film. However, the lowest thickness here is 0.3 ± 0.1 ML. It is reasonable to assume that at this ML value the coverage is incomplete. With patches of bare substrate exposed the HCA should be very low, as hexadecane will fully wet those areas, which will decrease the overall static contact angle. The next sample is of thickness 0.5 ± 0.1 ML. This is very close to the ML value proven to have complete film coverage, so the jump in the HCA can be attributed to the lack of any exposed silica. However, the fact that the HCA continues to rise between 0.5 ML to 0.7 ML, which seems to stress the importance of the film thickness for the wetting behavior of the film with respect to hexadecane. On the other hand, there remains no correlation between the IL film and the WCA. The WCA remains very low for all thickness values, on average $5.33^\circ \pm 3.91$ (shown in Figure 21 as the black line). While there are slight increases in the WCA at the lowest and highest thickness values recorded, since the contact angle never went past 15° in effect all the samples were fully wetted by water. So while there is a connection between film thickness and HCA, there is nothing similar for the WCA. Overall EMIIIm thin film on silica substrate does exhibit simultaneous hydrophilicity/oleophobicity for a wide range of film thickness values and surface topographies.

Even partial coverage still had the HCA greater than the WCA. The correlation of HCA with film thickness, and the constant WCA, seem to suggest that the wetting mechanism is dependent on the size of both the film and the contact liquid molecule. To test this theory, it is helpful to review a study where a similar phenomenon was observed. A final note: the advancing and receding contact angle was measured for EMIIIm thin film. The results are shown in [Appendix C](#).

The vast difference in static contact angle data between water and hexadecane and the dependence of HCA on film thickness seems to indicate that there is a size dependent mechanism of wettability of the film. An earlier study on the wettability of various PFPE thin film on silica observed that the contact liquid was penetrating the film²³. A ZDOL film on silica was found to exhibit simultaneous hydrophilicity/oleophobicity. To understand this behavior, the molecular arrangement of the film was analyzed. The film is essentially a net of polymer chains; the hydroxyl group at the end of the polymer chain would be bound to the substrate due to hydrogen bonding, and the fluorinated backbone would be arranged near the surface. This net of fluorine branches would repel both water and hexadecane. However, at the same time both liquids would be drawn to the high energy substrate. Both water and hexadecane would pass through the intermolecular holes in the film, going from the unfavorable fluorinated film surface to the favorable substrate. Due to the size difference between water and hexadecane the rate at which the liquid penetrated the film varied greatly. A water molecule is small compared to hexadecane; the size of a water molecule is 0.275 nm³⁰. and estimating the size of hexadecane using the ML formula yields 0.788 nm. Hence, water can pass through the film in little time, so the WCA is low and does not change with time. Hexadecane is larger, so the initial contact angle is high since hexadecane is being repelled by the fluorinated backbone. As time passes the

hexadecane passes through the film, seen in the way the HCA gradually decrease over time. This mechanism was confirmed by testing other PFPE films. A film of Z-03 lacks the hydroxyl end group of ZDOL, so the intermolecular holes will be larger due to the weaker bond between the polymer and the substrate. Because of this both water and hexadecane penetrate the film instantly, with no change in the contact angle over time. The same was true for Z-tetraol. The extra hydroxyl end group created a stronger bond with the substrate, resulting in a more ordered film and thus smaller intermolecular holes. Now both the WCA and HCA are constant because neither molecule can penetrate the film ²³. Last, the rate of film penetration by hexadecane was heavily influenced by the film thickness. The rate was about forty times slower when the film thickness was doubled ²⁰. The low WCA values obtained thus far prove the film has some intermolecular holes; in the absence of such gaps in the film the WCA would have been higher as water would have been repelled by the fluorinated branches on the surface. Combined with the brief change in HCA with film thickness and it is reasonable to test EMIIIm thin film for change in HCA over a long period of time.

To see whether the same film penetration mechanism present in ZDOL thin film might be at work in EMIIIm thin film, time-dependent HCA experiments were conducted. Trials were done for EMIIIm thin films of thickness 0.3, 0.5, 0.6, and 0.7 ± 0.1 ML, as well as bare PTFE. For each trial a drop of hexadecane was lowered onto the film. The contact angle of the hexadecane droplet was measured at 1-hour time intervals over the course of 24 hours for several EMIIIm films. The results are shown in Figure 22.

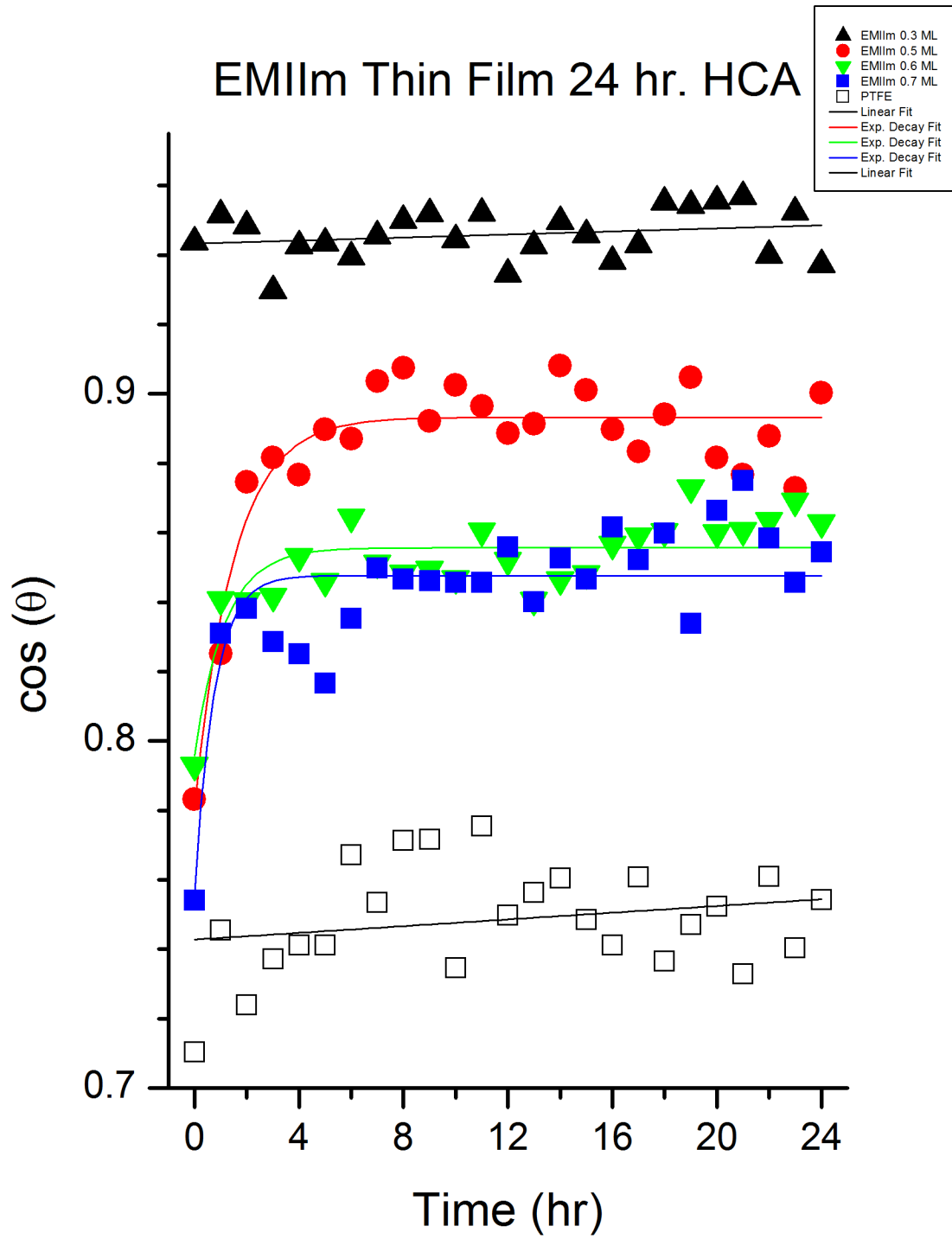


Figure 22: 24-hour HCA data trend for EMIIm thin film, with exponential fit, linear trendline (0.3 ML), and PTFE control trend with linear trendline

The data points used are an average of the left and right contact angles obtained for each hourly measurement. The contact angle data was plotted as the cosine of the angle over time and fitted to an exponential decay model:

$$[\cos(\theta)](t) = y_0 + A * \exp\left(-\frac{t}{\tau}\right)$$

The idea to use convert the data to $\cos(\theta)$ and model it using exponential decay was obtained from the ZDOL study. In that study the data was fitted using a modified Kohlrausch-Williams-Watts model (KWW):

$$[\cos(\theta)](t) = \cos(\theta_e) + (\cos(\theta_0) - \cos(\theta_e)) \exp\left[-\left(\frac{t}{\tau}\right)^\beta\right]$$

The main difference was the use of a power variable to modify the time t and the relaxation time constant τ . Trying to fit the 24-hour data to a KWW model failed, so an exponential decay model was used instead. The data for PTFE and 0.3 ML EMIIIm film had a poor fit to the decay model as well; these two sets of data were found to fit linear models with very low slopes, close to zero. The data for the other three films shows that the $\cos(\theta)$ increases to a constant value after 3 hours and remain constant for the rest of the trial. The slope of the three films ($1/\tau$), the “equilibrium” $\cos(\theta)$ reached by all samples, and the equivalent HCA in degrees, are all shown in Table 5.

Table 5: 24-hour HCA Exponential Fit Parameters

Film Thickness (± 0.1 ML)	0.5	0.6	0.7
Rate Constant $1/\tau$	0.68	0.87	1.33
Equilibrium $\cos(\theta)$	0.8933	0.8557	0.8477
Equilibrium HCA ($\pm 0.01^\circ$)	26.71	31.16	32.04

These three films (0.5, 0.6, and 0.7 ± 0.1 ML) show a clear decrease in HCA over time. This supports the hypothesis that the hexadecane is penetrating the film over time. The fact that the HCA for PTFE was nearly constant for the 24-hour trial supports the reliability of the data. Another trend apparent in the data is the fact that the HCA levels out after about 3 hours to an “equilibrium” HCA. The final HCA value also correlates with film thickness, with the final HCA increasing with film thickness. This too supports the penetration theory. The increase in the final HCA can be attributed to an increase the presence of anions/fluorinated branches as the film thickness increase. This will drive up the force repelling the hexadecane, leading to an increase in the final HCA as the thickness increases. In effect the final HCA is indeed an equilibrium HCA; the droplet will reach an equilibrium when the energy driving the film penetration matches the repulsion of the fluorinated anions. In the case of the 0.3 ML nm film the equilibrium HCA is the lowest due to the incomplete coverage of the IL film on the substrate. This also explains why there is no change in the HCA like for the other films: there is barely any film for hexadecane to penetrate, so the HCA will remain constant over time. The odd piece of data obtained is the trend of the rate constant $1/\tau$. Unlike ZDOL the rate seems to increase with film thickness. This seems to correlate with the trend of the “equilibrium” HCA; the rate seems to increase only because there is less difference between the initial and final HCA. While this makes sense mathematically it does defy basic mass transfer principle. Comparing the values of the decay model and the experimental data, it can be seen that the major flaw with the model is that it yields a very different initial contact angle than the experimental data, at least for two of the data sets. This, combined with the subpar R^2 fit for each of the data sets suggest that the model is flawed. This would mean that IL film penetration follows a rather different kinetic path than the ZDOL film penetration. This makes sense when comparing the forces that drive the

formation of the films. ZDOL thin film is formed by hydrogen bonding between the end group and the substrate. EMIIIm thin film is formed via a weak electrostatic interaction that drive alternating layers of ions. This means that the intermolecular network will be very different for the two films, leading to different kinetic behavior. The thermodynamics of the two systems remains the same, as seen by how the model yields an equilibrium HCA value very close to the experimental data trend.

As seen in the 24-hour data the HCA reaches an equilibrium after about 3 hours for all of the films with a change in HCA. To attempt to clarify the data trend 3-hour HCA time trials were conducted. The results are shown in Figure 23, using the same exponential decay model as in Figure 23; the rate constant of the three films ($1/\tau$), the equilibrium $\cos(\theta)$ reached by all samples, and the equivalent HCA in degrees, are all shown in Table 6.

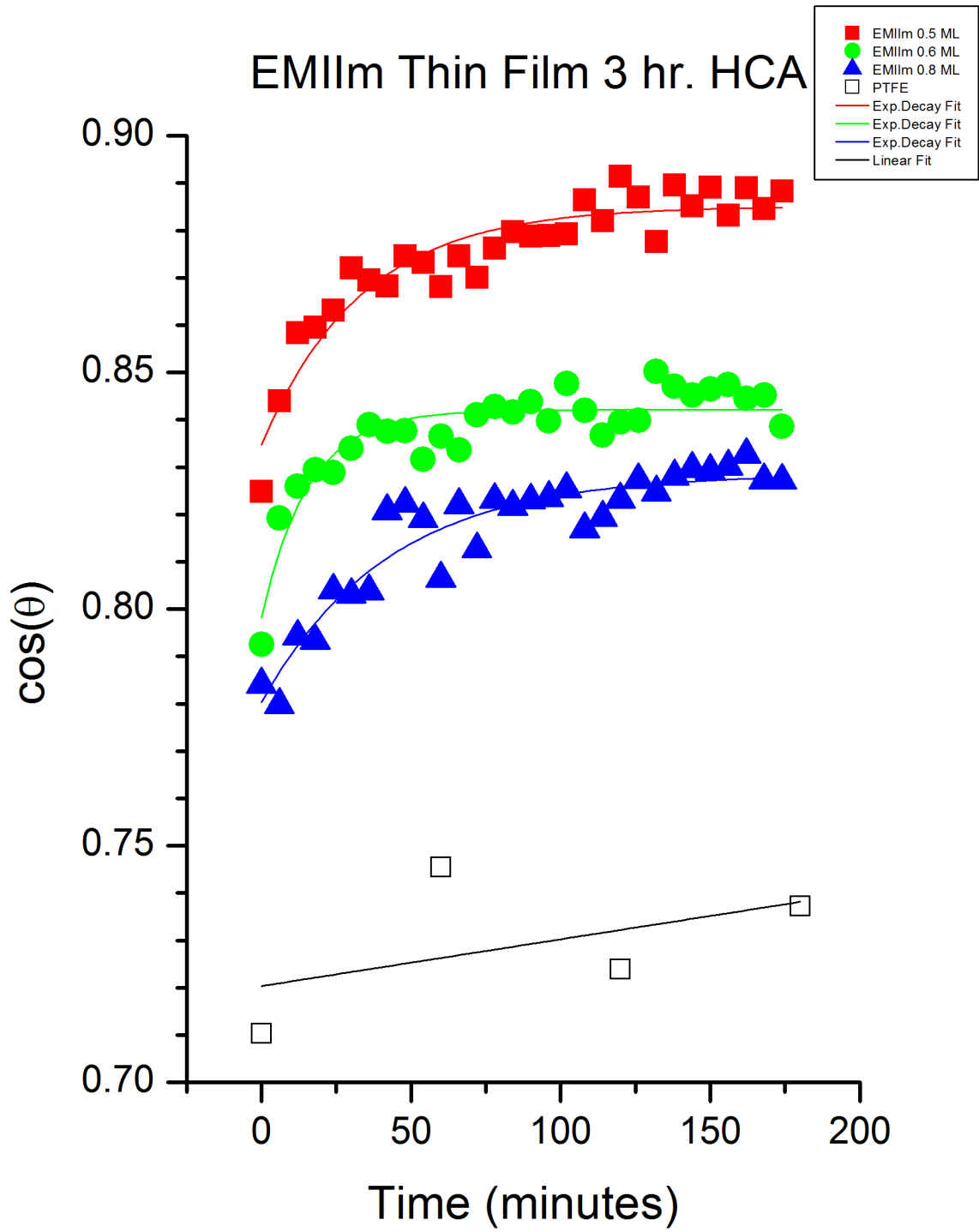


Figure 23: 3-hour HCA data trend for EMIIm thin film, with exponential fit and PTFE control trend

Table 6: 3-hour HCA Exponential Fit Parameters

Film Thickness (± 0.1 ML)	0.5	0.6	0.8
Rate Constant $1/\tau$	0.0299	0.0636	0.0238
Equilibrium $\cos(\theta)$	0.8848	0.8421	0.8277
Equilibrium HCA ($\pm 0.01^\circ$)	27.77	32.64	34.14

The data points used are an average of three different three-hour trials conducted on three different samples. The trend is the same as for the 24-hour data. For all the films tested the HCA decreases to an equilibrium value over 3 hours. The equilibrium HCA remains dependent on the film thickness, with the value increasing with the thickness. This data set further supports the theory that wetting of EMII thin film is controlled by kinetics, dependent on the film thickness. Unfortunately, a model of the kinetics continues to be elusive. The 3 hr. data fit the exponential delay model better, with an average R^2 value of 0.8933; this is apparent in the accuracy of the initial and final HCA. However, there is still no correlation between the film thickness and a rate constant. This also seems to confirm that the kinetics of the wetting of EMII thin film is very unique, requiring rigorous mathematical analysis to model properly.

5.0 CONCLUSION

An important field in wettability research is designing simultaneously oleophobic/hydrophilic surfaces. Such surfaces not only prevent fogging but also repel hydrocarbon contaminants in the environment, giving them a longer life-span over traditional anti-fogging coatings and surfaces. The current study demonstrates that a EMIIIm thin film on silicon wafer shows simultaneously oleophobic/hydrophilic behavior.

EMIIIm thin film samples were created by dip coating. Before conducting wettability tests the EMIIIm film topography was analyzed by optical microscope, tapping mode AFM, ellipsometry, and ARXPS. Optical and AFM images showed dewetting on the films of certain samples; as the solution concentration used to create the samples was decreased, the severity of the dewetting was also decreased. Ellipsometry data showed that there was a critical film thickness at which point the film would start to see dewetting. This critical value was verified via optical images, AFM section analysis, and variations in ellipsometry data collection. The arrangement of the ions was analyzed using ARXPS. ARXPS results showed that for thin films without dewetting there is anion/cation layering, with the fluorinated anions close to the film surface.

Initial contact angle testing of EMIIIm thin film on silica showed that static HCA is higher than the static WCA, indicating that the film is simultaneously oleophobic/hydrophilic. Given the size difference between hexadecane and water it was hypothesized that the contact angle was

kinetically determined, and there was penetration of the testing liquid through the film. This was confirmed in time-dependent HCA trials of various EMIm thin films. By monitoring the HCA value over a 24-hour time period it was confirmed that film penetration was occurring as the HCA decreased over time to a final equilibrium value; the final HCA value was dependent on the film thickness.

There remains much work to be done in IL thin film wettability. The obvious next step is to analyze the wettability of an IL film with few or no fluorinated bonds, such as 1-Butyl-3-Methylimidazolium TetraFluoroborate (BMImBF₄). The high HCA is supposed to be due to the heavily fluorinated film surface, so by decreasing the amount of fluorinated branches at the surface the HCA should decrease, or should decrease faster over time. A related follow-up study is changing the cation. EMIm and DMPIIm had different interactions with the silica substrate due to a simple change in the alkyl side chains in the cation. Changing the interaction will change the molecular arrangement; beyond determining at what thickness film dewetting will occur, changing the molecular arrangement will change the intermolecular “holes” in the film, which should change the rate of film penetration. This can also be done by changing the substrate used. A substrate with a higher surface charge, such as mica, should result in a more tightly bound film, which should decrease the rate film penetration. In addition, the ionic liquid-substrate interaction can also be manipulated by introducing surfactants to the system. The presence of alumina or other surfactants can drive the ions to either bind to the surfactant or bind irregularly to the substrate, as the ions now compete with the surfactant for space on the substrate. Finally, it would be worth exploring the effect of the dip coating speed and dwell time on IL thin film formation. Theoretically neither should have much effect since IL film formation is dependent on electrostatic attraction to the substrate, not full binding (i.e. hydrogen

bonding or dipole interaction). This might change depending on the ionic liquid and substrate used.

APPENDIX A

ELLIPSOMETRY DATA FOR EMIIIM THIN FILM

Table 7: Ellipsometry Data for EMIIIm Solution 0.01, 0.1, 0.2, 0.25 g/L

EMIIIm Solution Concentration (g/L)							
0.01		0.1		0.2		0.25	
Thickness (nm)	MSE	Thickness (nm)	MSE	Thickness (nm)	MSE	Thickness (nm)	MSE
0.31	2.994	0.41	3.255	0.41	1.611	0.55	2.984
0.28	3.580	0.42	3.208	0.41	1.574	0.55	3.058
0.28	3.962	0.41	2.590	0.41	1.569	0.54	2.905
0.26	2.835	0.41	3.071	0.40	1.655	0.54	2.867
0.26	3.176	0.42	2.951	0.42	1.574	0.55	2.867
0.21	1.452	0.36	1.586	0.44	1.432		
0.21	1.470	0.36	1.614	0.44	1.505		
0.21	1.519	0.36	1.489	0.45	1.525		
0.22	1.542	0.35	1.735	0.44	1.541		
0.22	1.563	0.35	1.548	0.45	1.572		

Table 8: Ellipsometry Data for EMIIm Solution 0.3, 0.5, 0.75 g/L

EMIIm Solution Concentration (g/L)					
0.3		0.5		0.75	
Thickness (nm)	MSE	Thickness (nm)	MSE	Thickness (nm)	MSE
0.55	1.350	0.90	2.735	1.07	3.520
0.53	1.399	0.90	3.053	1.06	3.362
0.56	1.365	0.95	2.822	1.08	3.530
0.55	1.385	0.91	3.147	1.06	3.380
0.53	1.380	0.91	3.212	1.07	3.360
0.58	2.613	0.78	2.086		
0.60	1.564	0.77	2.138		
0.59	1.613	0.78	2.382		
0.60	1.603	0.77	2.464		
0.61	1.571	0.76	2.322		

Table 9: Ellipsometry Data for EMIIm Solution 1.0, 5.0 g/L

EMIIm Solution Concentration (g/L)			
1.0		5.0	
Thickness (nm)	MSE	Thickness (nm)	MSE
1.23	3.442	3.66	27.331
1.24	3.594	3.35	26.051
1.27	3.786	3.30	25.859
1.22	3.811	3.33	26.619
1.23	4.062	3.31	26.438
1.30	3.636		
1.34	3.689		
1.30	3.840		
1.30	3.821		
1.38	4.333		
1.31	4.107		
1.28	4.184		
1.28	4.410		

APPENDIX B

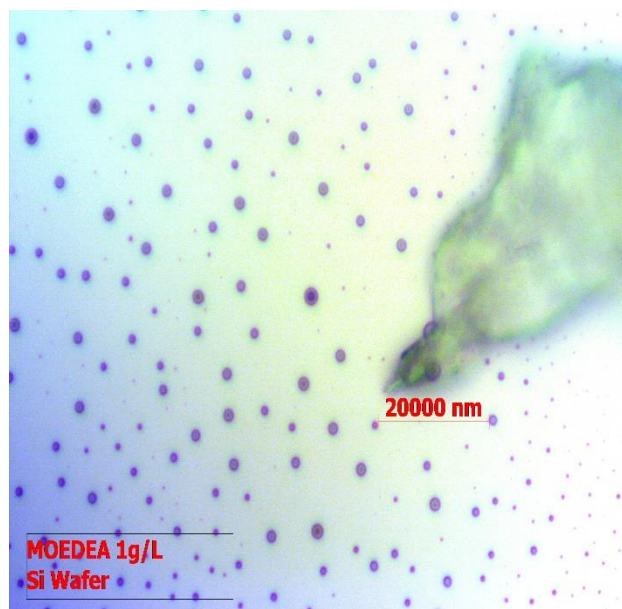
TOPOGRAPHY OF IONIC LIQUID THIN FILMS

The average film thickness of MOEDEA, EMZIA, and EMIIIm thin film made from solutions of 1 g/L are listed in Table 10. The same Cauchy model was used for all three thickness measurements.

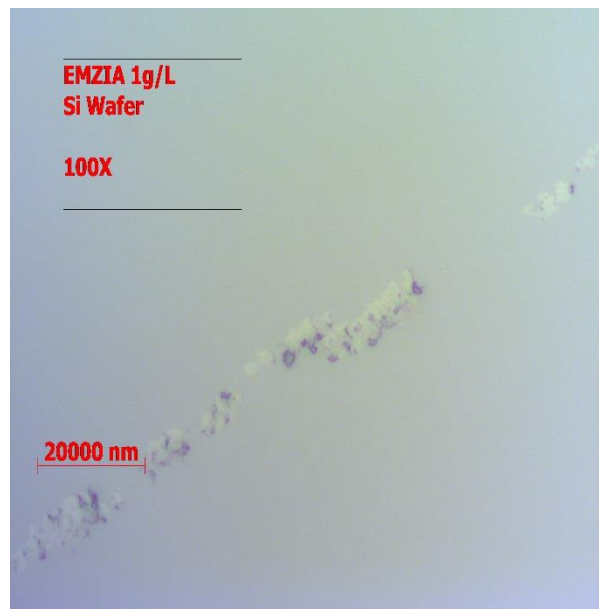
Table 10: Film Thickness for MOEDEA, EMZIA, and EMIIIm, for 1.0 g/L

Ionic Liquid, 1.0 g/L	Average Film Thickness (nm) Cauchy Model A= 1.45, B=0.01, C=0
MOEDEA	1.36 \pm 0.159
EMZIA	0.91 \pm 0.167
EMIIIm	1.28 \pm 0.046

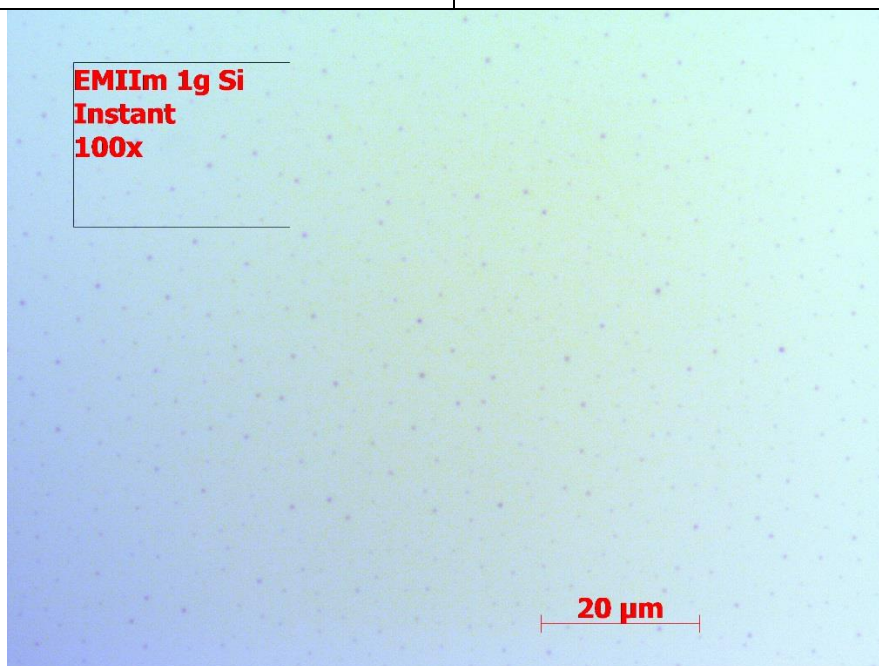
Optical images were taken of film samples of MOEDEA, EMZIA, and EMIIIm on silicon wafer, all made from solutions of 1 g/L. The optical images are shown in Figure 24. While MOEDEA and EMIIIm showed signs of dewetting EMZIA did not. To investigate this further AFM scan were done on the three samples.



MOEDEA 1 g/L



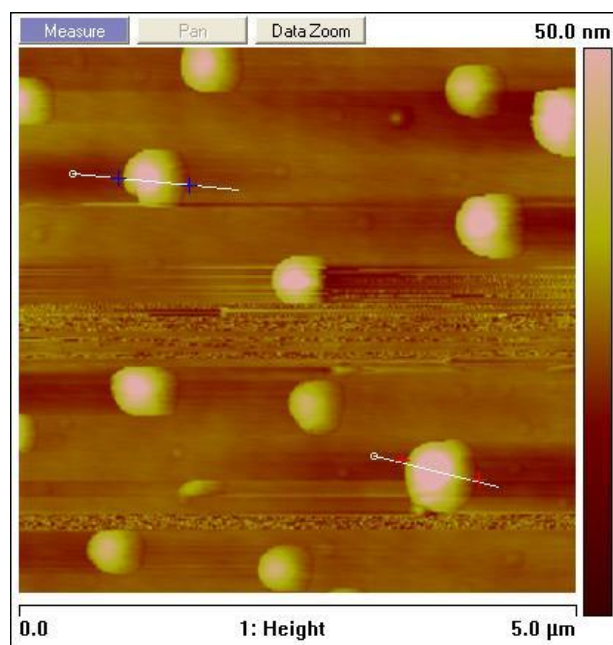
EMZIA 1 g/L



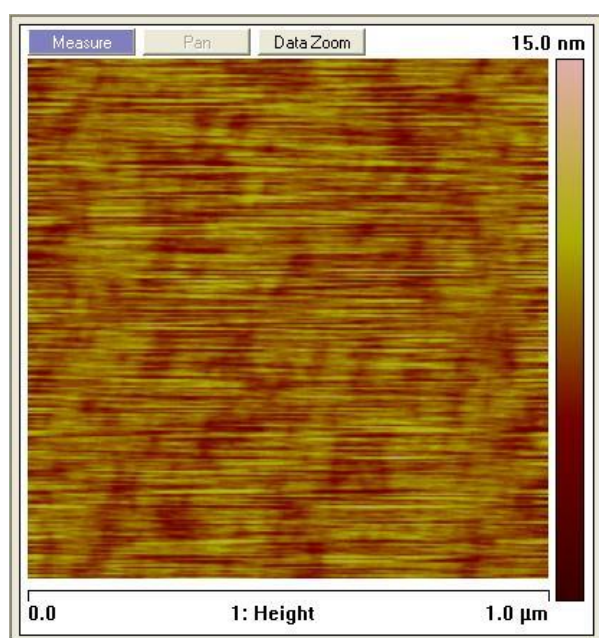
EMIIIm 1 g/L

Figure 24: Optical images of MOEDEA, EMZIA, and EMIIIm film on silicon wafer, all solution 1 g/L

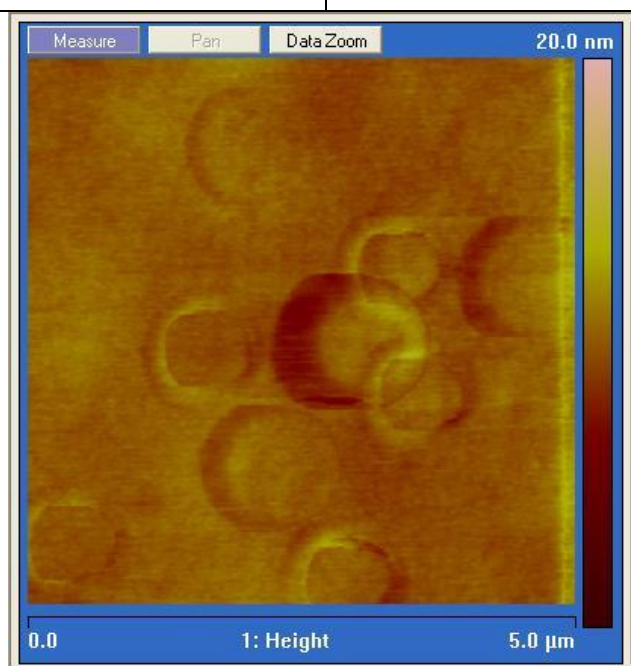
Dewetting was further confirmed via AFM topography images, seen in Figure 25. The droplets on the MOEDEA film were very well defined and very prominent on the film, reaching an estimated height of 10.0 ± 0.1 nm from the film. In contrast EMZIA did not show any sign of dewetting despite the high concentration used. A structure analysis can at least explain the severe dewetting seen for MOEDEA. Unlike EMIIIm or EMZIA the MOEDEA cation is an ammonium, a nitrogen with four bonds. The cation is restricted to a tetrahedral shape, and the ethyl and ester branches will cause even more steric hindrance when it comes to packing. As such MOEDEA should almost exclusively favor bulk arrangement, since it cannot interact effectively with the substrate; instead of layer growth MOEDEA seems to exhibit droplet growth, leading to the very prominent drops seen in optical and AFM images. The lack of dewetting on EMZIA can also be explained via sterics. Though it shares the same cation with EMIIIm EMZIA has an anion which is far bulkier. While the cation can easily form a layer the anion should have difficulty arranging into a layer. Notice though that instead of dewetting the EMZIA film appears as a sponge-like film, with spots of less film coverage. It would seem that a bulky anion alone does not promote dewetting. So long as the cation can align with the substrate it will favor layer formation. The bulk anion only breaks up the layer, preventing a single smooth layer like for EMIIIm. This would also explain why EMZIA has a high thickness when made using 1.0 g/L solution but does not exhibit dewetting. Layers do build but they are broken up by the bulk anion. This prevents screening of the substrate, so cation layering can continue even at higher thickness.



MOEDEA 1 g/L



EMZIA 1 g/L



EMIIIm 1 g/L

Figure 25: AFM Topography images of MOEDEA, EMZIA, and EMIIIm film on silica, all solution 1 g/L

APPENDIX C

DYNAMIC CONTACT ANGLE ANALYSIS OF EMIIIM THIN FILM

A final test of the film structure was the measurement of the advancing contact angle of 0.6, 1.1, and 1.7 ML films. The advancing HCA values obtained are shown in Table 11.

Table 11: Advancing HCA for EMIIIm thin film on silica

Film Thickness (± 0.1 ML)	Advancing HCA (degree, $\pm 0.01^\circ$)
0.6	55.00 ± 2.40
1.1	55.90 ± 6.79
1.7	53.55 ± 7.42

To verify that the advancing HCA was taken at the proper time, a graph of HCA over dispensing time was constructed. This graph is shown in Figure 26; the data points are an average of three trials.

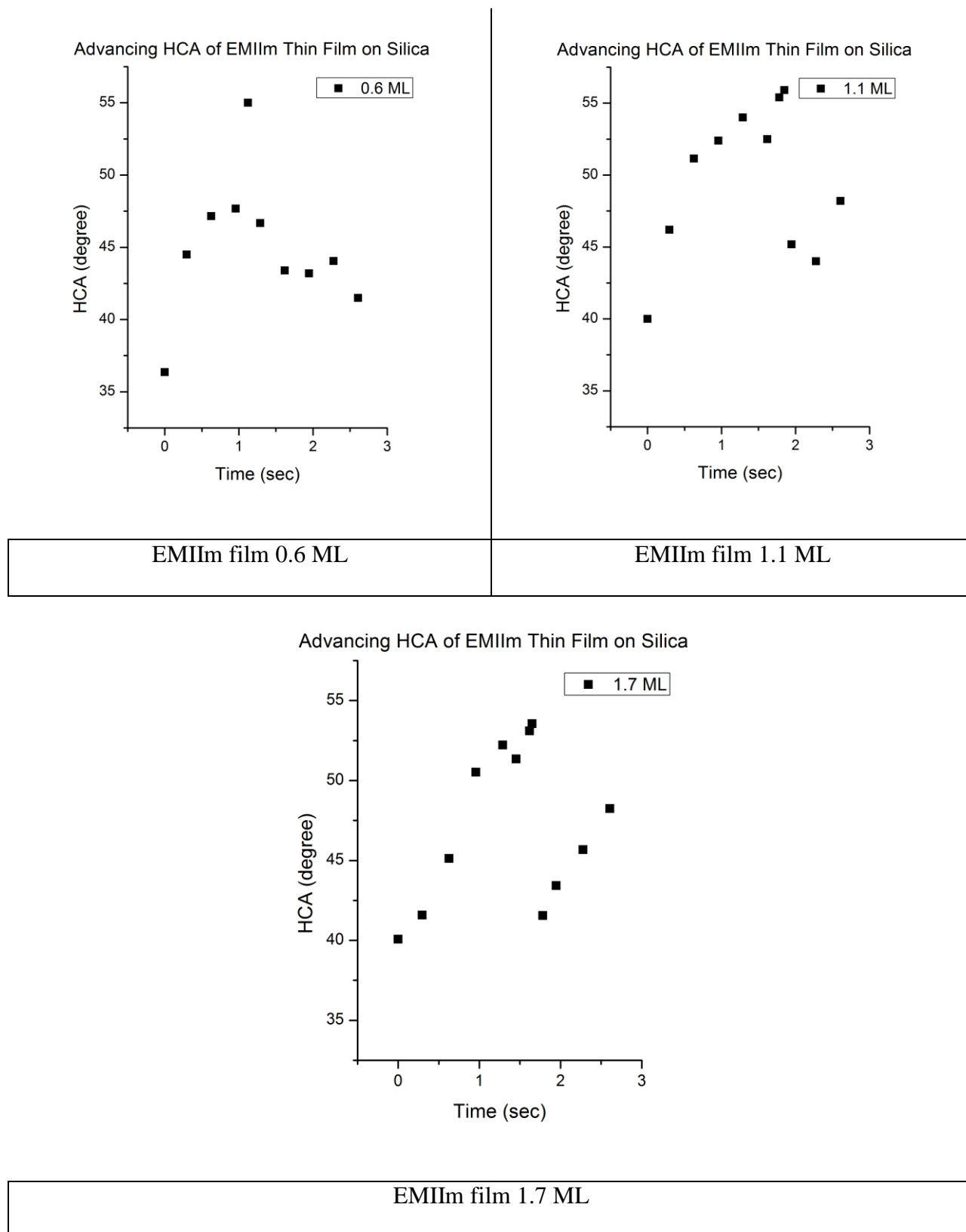


Figure 26: Advancing Contact Angle graphs for EMIIIm film

It seems that the advancing HCA is very similar for all three films. The similar advancing HCA suggests a common surface topography. Based on the AFM analysis this should be because all three samples show complete film coverage. Moreover, if there were patches of exposed substrate then there would be a huge spike in the advancing HCA, as the hexadecane droplet would be drawn to the substrate. The advancing HCA is relatively low, only about 15° more than the average static HCA. This is due to the presence of the fluorinated branches on the film surface. The fluorinated branches repel hexadecane, so there is a drive to seek a more favorable configuration to minimize the total energy. The fact that dewetting does not affect the advancing HCA confirms that the bulk arrangement is partially arranged into layers, as seen in the ARXPS analysis. If the droplets on the film were purely random arrangement, then the advancing HCA should decrease. A random arrangement would mean that the droplets would be covered in equal parts cation and anion, as opposed to the layered structure which emphasizes the anion on the surface. The hexadecane would be drawn to these droplets since there would be less repulsion compared to the fluorinated anion film. Hence the advancing HCA would decrease. With partial layering there is less of a drive for the hexadecane to move towards the droplets so the advancing HCA remains unchanged.

Receding HCA was also taken for 0.6 and 1.1 ML EMIIIm film. The graph of receding HCA is shown in Figure 27; the data was taken from two trials, for contact angles measured from an initial droplet volume of $3.0\ \mu\text{L}$.

Receding HCA of EMIIIm Thin Film on Silica

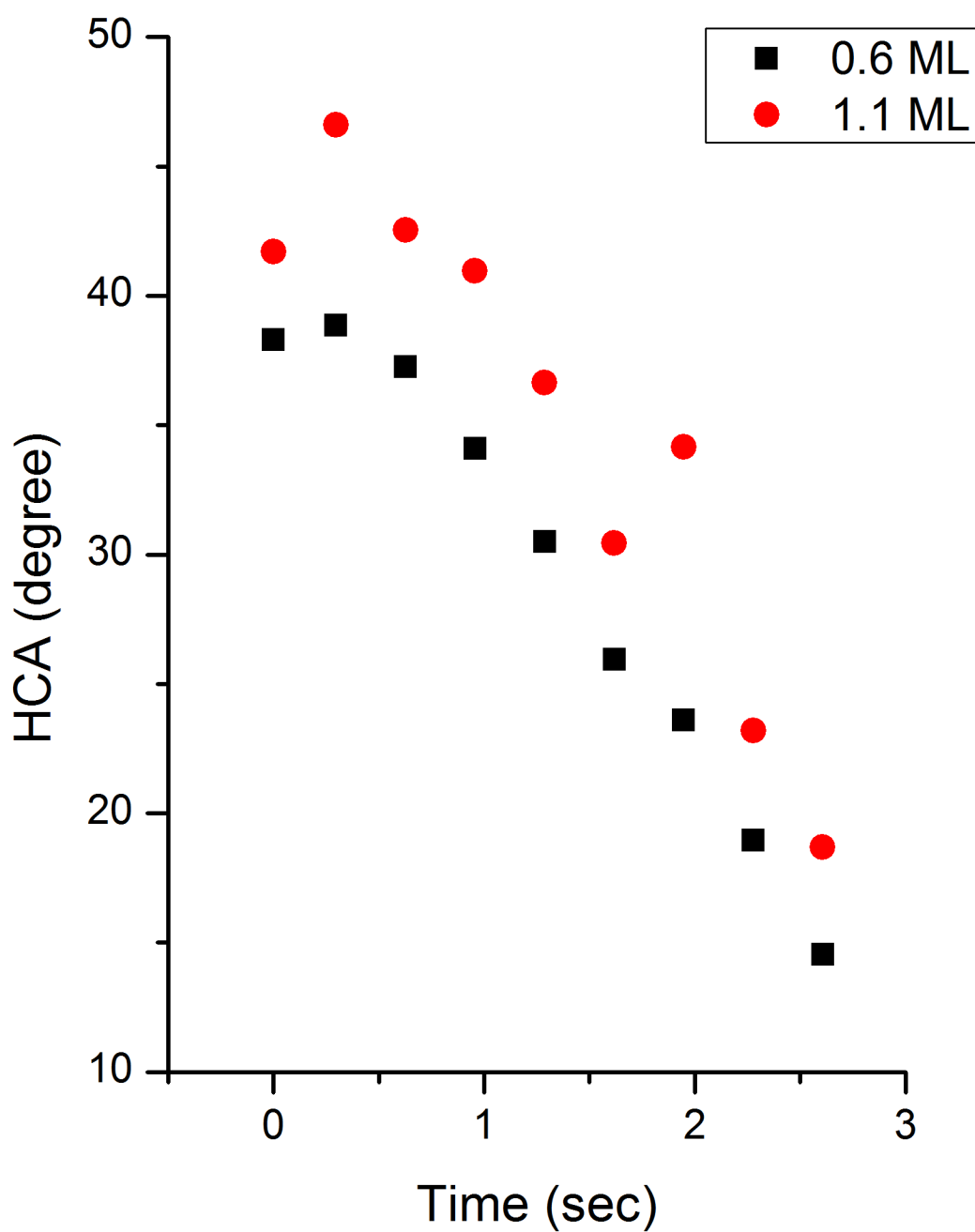


Figure 27: Receding HCA for EMIIIm film 0.6, 1.1 ML

In experimental observation there was no clear change in the droplet shape (i.e. no “jump” as the droplet decreased in size). This observation, or lack thereof, was noted for initial hexadecane droplets of 2.5, 3.0, and 4.0 μL . Graphing the receding HCA data does not reveal a minimum HCA; for both data sets there is a linear decrease in the HCA from the start of the trial to the end. Thus far there is no satisfactory explanation why this is the case. Shape change should be almost immediate since the surface is repelling hexadecane. Perhaps using a different technique to measure contact angle, such as Wilhelmy plate, would be able to capture the receding contact angle.

Finally, advancing and receding WCA was taken, but in all trials conducted the angle was always too low to measure. As such no data has been reported.

BIBLIOGRAPHY

1. Holbrey, J.D. and R.D. Rogers, *Green Industrial Applications of Ionic Liquids: Technology Review*, in *Ionic Liquids*. 2002, American Chemical Society. p. 446-458.
2. Hayes, R., G.G. Warr, and R. Atkin, *Structure and Nanostructure in Ionic Liquids*. Chemical Reviews, 2015. **115**(13): p. 6357-6426.
3. Lu, D., N. Shomali, and A. Shen, *Task specific ionic liquid for direct electrochemistry of metal oxides*. Electrochemistry Communications, 2010. **12**(9): p. 1214-1217.
4. Kim, K.-I., et al., *Fabrication of a Multi-Walled Nanotube (MWNT) Ionic Liquid Electrode and Its Application for Sensing Phenolics in Red Wines*. Sensors, 2009. **9**(9): p. 6701.
5. Endres, F., et al., *Do solvation layers of ionic liquids influence electrochemical reactions?* Physical Chemistry Chemical Physics, 2010. **12**(8): p. 1724-1732.
6. Welton, T., *Room-Temperature Ionic Liquids. Solvents for Synthesis and Catalysis*. Chemical Reviews, 1999. **99**(8): p. 2071-2084.
7. Wasserscheid, P. and W. Keim, *Ionic Liquids—New “Solutions” for Transition Metal Catalysis*. Angewandte Chemie International Edition, 2000. **39**(21): p. 3772-3789.
8. Chauvin, Y., L. Mussmann, and H. Olivier, *A Novel Class of Versatile Solvents for Two-Phase Catalysis: Hydrogenation, Isomerization, and Hydroformylation of Alkenes Catalyzed by Rhodium Complexes in Liquid 1,3-Dialkylimidazolium Salts*. Angewandte Chemie International Edition in English, 1996. **34**(23-24): p. 2698-2700.
9. Song, C.E. and E.J. Roh, *Practical method to recycle a chiral (salen)Mn epoxidation catalyst by using an ionic liquid*. Chemical Communications, 2000(10): p. 837-838.
10. Hayes, R., G.G. Warr, and R. Atkin, *At the interface: solvation and designing ionic liquids*. Physical Chemistry Chemical Physics, 2010. **12**(8): p. 1709-1723.
11. Kamimura, H., et al., *Effect and mechanism of additives for ionic liquids as new lubricants*. Tribology International, 2007. **40**(4): p. 620-625.

12. Howarter, J.A. and J.P. Youngblood, *Self-Cleaning and Next Generation Anti-Fog Surfaces and Coatings*. Macromolecular Rapid Communications, 2008. **29**(6): p. 455-466.
13. Israelachvili, J.N., *Intermolecular and surface forces: revised third edition*. 2011: Academic press.
14. Perkin, S., T. Albrecht, and J. Klein, *Layering and shear properties of an ionic liquid, 1-ethyl-3-methylimidazolium ethylsulfate, confined to nano-films between mica surfaces*. Physical Chemistry Chemical Physics, 2010. **12**(6): p. 1243-1247.
15. Perkin, S., et al., *Self-assembly in the electrical double layer of ionic liquids*. Chem Commun (Camb), 2011. **47**(23): p. 6572-4.
16. Gong, X., A. Kozbial, and L. Li, *What causes extended layering of ionic liquids on the mica surface?* Chemical Science, 2015. **6**(6): p. 3478-3482.
17. Gong, X., et al., *Thickness-dependent molecular arrangement and topography of ultrathin ionic liquid films on a silica surface*. Chem Commun (Camb), 2013. **49**(71): p. 7803-5.
18. Bracco, G. and B. Holst, *Surface science techniques*. 2013: Springer Science & Business Media.
19. Extrand, C.W. and Y. Kumagai, *An Experimental Study of Contact Angle Hysteresis*. Journal of Colloid and Interface Science, 1997. **191**(2): p. 378-383.
20. Li, L., et al., *Why can a nanometer-thick polymer coated surface be more wettable to water than to oil?* Journal of Materials Chemistry, 2012. **22**(33): p. 16719.
21. Lampitt, R.A., J.M. Crowther, and J.P.S. Badyal, *Switching Liquid Repellent Surfaces*. The Journal of Physical Chemistry B, 2000. **104**(44): p. 10329-10331.
22. Howarter, J.A. and J.P. Youngblood, *Self-Cleaning and Anti-Fog Surfaces via Stimuli-Responsive Polymer Brushes*. Advanced Materials, 2007. **19**(22): p. 3838-3843.
23. Wang, Y., et al., *Effect of end-groups on simultaneous oleophobicity/hydrophilicity and anti-fogging performance of nanometer-thick perfluoropolyethers (PFPEs)*. RSC Adv., 2015. **5**(39): p. 30570-30576.
24. Mittal, K., *Surface contamination: an overview*, in *Surface contamination*. 1979, Springer. p. 3-45.
25. Tompkins, H. and E.A. Irene, *Handbook of ellipsometry*. 2005: William Andrew.

26. Co., J.A.W. 2016 [cited 2016 June 24]; Available from: <https://www.jawoollam.com/resources/ellipsometry-tutorial/ellipsometry-measurements>.
27. Mironov, V.L., *Fundamentals of scanning probe microscopy*. Moscow: Technosfera, 2004: p. 144.
28. van der Heide, P., *X-ray Photoelectron Spectroscopy : An introduction to Principles and Practices (1)*. 2011, Hoboken, US: Wiley.
29. Rollins, J.B., B.D. Fitchett, and J.C. Conboy, *Structure and Orientation of the Imidazolium Cation at the Room-Temperature Ionic Liquid/SiO₂ Interface Measured by Sum-Frequency Vibrational Spectroscopy*. The Journal of Physical Chemistry B, 2007. **111**(18): p. 4990-4999.
30. Zhang, Y. and Z. Xu, *Atomic radii of noble gas elements in condensed phases*. American Mineralogist, 1995. **80**(7-8): p. 670-675.